Influence of Si- and W- doping on micro-scale reciprocating wear and impact performance of DLC coatings on hardened steel

Ben D. Beake[1,*], Sam J. McMaster[2], Tomasz W. Liskiewicz[3], and Anne Neville[2]

1 Micro Materials Ltd, Willow House, Yale Business Village, Ellice Way, Wrexham, LL13 7YL, United Kingdom

2 Institute of Functional Surface, School of Mechanical Engineering, University of Leeds, Woodhouse Lane, Leeds LS2 9JT, United Kingdom

3 John Dalton Building, Faculty of Science and Engineering, Manchester Metropolitan University, Chester Street, Manchester M15 6BH, UK

*Corresponding author: Tel: +44 1978 261615; e-mail: ben@micromaterials.co.uk

Abstract

Reciprocating micro-scale sliding tests and micro-scale repetitive impact tests were performed with diamond probes on un-doped, Si-doped and W-doped diamond-like carbon (DLC) coatings on hardened steel with a nanomechanical test instrument. Analytical modelling showed that differences in coating behaviour during sliding contact could be interpreted by differences in the stress distribution that develops. The softer W-doped DLC exhibited the lowest wear resistance in reciprocating sliding. The deformation in the wear track under the test conditions (R = 25 μm, $P \leq$ 500 mN, total sliding distance = 1 m) was largely controlled by plastic deformation and hence hardness, since micro-scale fatigue wear was only a small contributor. The relationship between friction and wear was more complex, due to the changing influence of surface topography, asperity ploughing and wear with increasing reciprocating sliding cycles. The Si-doped DLC showed the lowest resistance to repetitive impact. The hardest and highest H^3/E^2 coating, un-doped DLC, was also

susceptible to fracture throughout the load range. Although the W-doped DLC was the softest coating studied and had low wear resistance in reciprocating sliding, it was significantly more damage tolerant to repetitive impacting than the other coatings despite its low hardness and low wear resistance in reciprocating tests.

Keywords: Diamond-like carbon; Micro-/Nano-scale Friction; Ploughing; Impact

1. Introduction

Deformation and wear begins at the asperities between contacting surfaces [1-5] but the contact pressures acting on these are not generally accurately known in a macro-scale tribological test with multi-asperity contact. The contact zone is hidden and the real area of contact is initially a small fraction of the apparent contact area [3,4,6]. The actual contact pressure during the running-in phase is therefore significantly higher than the nominal calculated Hertzian pressure. The simplified contact conditions in single asperity tribological tests with much lower forces and sharper probes provide an alternative approach to study the onset of wear, its correlation with friction, and the influence of surface topography and mechanical properties. [4-5,7-8] With their small radius probe tips, higher resolution and low noise floor atomic force microscopes (AFMs) have been used for single asperity tribological tests [7,9], although there are certain limitations including (i) short track distances (ii) low sliding speed (iii) high contact pressures (iv) susceptibility to probe wear due to the small tip radius. TEM single asperity and MD approaches have also been used to study the onset of wear in single asperity contacts [8,10-12]. Another popular approach is to use a nanoindenter with typically larger probe radii (often in the micron range) and larger available force range to perform nano-scratch tests [13]. Contact pressures in ramped load nano-scratch tests are often necessarily high (due to the requirement to cause coating failure in a single cycle) and the ploughing component to the friction force can be relatively large. The contact pressure

remains high in a repetitive sub-critical load scratch test, where the conditions are chosen so that the peak stresses can be placed in the coating or in the vicinity of the interface. The test shows enhanced sensitivity to subtle differences in interfacial bonding strength [13], although the number of repeat cycles in the tests has been typically low.

Nanoindenters and microtribological instruments have been used by several researchers to study solid lubricant coating behaviour in reciprocating friction and wear tests at the mN force range [14-25]. Schiffmann studied the correlation between friction and the evolution of elastic, plastic deformation and wear in reciprocating testing of DLC and Si-doped DLC on glass. Stoyanov and co-workers studied the microtribological properties of Au, Au-MoS_2 composite and Au/MoS_2 bilayer coatings showing improved behaviour in reciprocating tests for the composite and bilayers, and ex-situ characterisation of the wear track revealing tribofilm formation [23-24]. Achanta and co-workers performed reciprocating sliding tests at different length scales and showed that the topographical influence on friction was significant at small scale contact [15,17,19]. At NPL Gee and co-workers developed a microtribometer that could be used as a bench top system or in an SEM [18,20]. Wilson and co-workers described a modular addition to a commercial nanoindenter with stability to run reciprocating (nano-fretting) tests to over 200000 cycles [21-22]. In the nano-fretting test the much larger number of cycles that can be conveniently run enables tests at lower stresses (via probes with larger radii and/or using smaller contact loads). The small track length means that total sliding distance is relatively low but the transition from fretting/partial slip to gross slip was studied in wear of amorphous carbon films [21-22].

An additional microtribology capability has been implemented in the same modular commercial nanoindenter and validated on biomedical alloys and sliding interconnector materials [26]. When electrically conductive probes were used improved detection of the onset of wear and the subsequent failure mechanisms was possible by a multi-sensing

approach simultaneously monitoring friction and electrical contact resistance. The larger sliding speeds and larger sliding distances than in other microtribological tests enable longer duration high or low contact pressure tests. Higher sliding speeds enable direct replication of those in MEMS contacts [27]. Table 1 (a) compares the typical conditions in the new capability for nano-scale reciprocating wear to AFM nano-wear and to other approaches for multi-pass sliding contacts with the same instrumentation.

In this work it has been used to study the micro-scale friction and wear of DLC coatings in reciprocating tests over sliding distances that were large in comparison to those normally used in micro-scale testing. Low friction diamond-like carbon (DLC) coatings are applied to many components in the automotive power train such as tappets, pistons, piston rings and fuel injectors [28-29]. Friction reduction in automotive engines reduces fuel and helps meet environmental and legislative requirements [30-32]. With power train trends to downsizing, turbocharging, low lubricant viscosity and start-stop the number of components operating in boundary/mixed lubrication regime will increase. Under boundary conditions the surface is critical to achieve low friction and wear. In several of these applications repetitive impact or impact-sliding may also occur [29]. Additional deformation mechanisms can occur in cyclic tests that are not observed in single loading tests [33-35]. A recently developed micro-impact test, using a diamond probe of similar sharpness to that used for the micro-scale reciprocating tests, can be used to study fracture resistance and damage tolerance.

The micro-scale reciprocating wear and repetitive impact tests have been used to investigate the performance of Si-doped and W-doped DLC coatings in comparison with a typical hard un-doped DLC. W-doped DLC has been shown to perform well in a wide range of tribological conditions [36]. Si-doped DLC has low friction and has been evaluated for a range of applications, although it has been noted that its wear resistance can be inferior to un-doped DLC [37]. Their behaviour in reciprocating nano-wear [25], nano-scratch and micro-

scratch tests [38] has been reported previously. Since their relative performance was found to be dependent on the testing conditions [25,38] it is of interest to study how they perform over longer sliding distances and higher sliding speeds, while maintaining the same probe geometry as in the micro-scratch tests. The relationship between wear and friction was investigated with support from simulated stress distributions. Their behaviour under repetitive impact was compared to tests on other carbon coatings [39] under the same experimental conditions to improve understanding of the role of coating mechanical properties on their damage tolerance. The differences in test probe geometry, applied load and number of cycles in the previous studies and the new reciprocating wear and micro-impact tests are summarised in Table 1 (b).

2. Experimental

2.1 Materials

Multilayer coatings with a-C:H (un-doped DLC) and Si-a-C:H (Si-doped DLC) top layers were deposited on hardened M2 tool steel with a PECVD Flexicoat 850 system (Hauzer Techno Coating, the Netherlands). a-C:H:W (W-doped DLC or WC/C) was a commercial coating, Balinit C Star, deposited on hardened M2 tool steel by Oerliken Balzers. According to the manufacturer specification, Balinit C Star is applied in a single-pass vacuum process at temperatures between 180 and 350 °C, resulting in a homogeneous coating with multilamellar structure with WC-rich/C-rich phases alternating every few atomic layers [40]. There is a hard CrN sub-layer for load support and improved adhesion to the steel substrate. EDX surface measurements on the commercial W-doped DLC coating showed 66.9 wt.% W, 25.2 wt.% C with a minor amount (5.3 wt. %) of Ni also present that was presumably residual contamination from a previous coating run. EDX surface composition was 95.0 wt.% C, 3.6

wt.% W for a-C:H and 67.5 wt.% C, 22.1 wt.% Si, 5.4 wt.% W and 3.5 wt. % O for Si-a-C:H. In the a-C:H and Si-a-C:H coating systems the adhesion layer is a 300 nm Cr and then gradient tungsten carbide layers are applied to adapt the elastic modulus of the soft substrate to the elastic modulus of the hard top coating, improving of the coating's ability to resist both abrasive and impact fatigue wear. The Cr layer was deposited using magnetron sputtering, while the WC layer was deposited using magnetron sputtering with the gradual introduction of Acetylene gas to the complete PACVD stage, thus creating a functional gradient layer in one continuous deposition process. The Si-a-C:H was doped with silicon using hexamethyldisiloxane (HDMSO) precursor. Thickness of the coatings was assessed by ball cratering (Calotester, Tribotechnic, France). Full details of the composition, thickness and mechanical properties of the coatings are shown in Table 1(a). In this publication the coatings are referred to by their top layer composition. Nanoindentation and micro-scratch tests were performed using the NanoTest Vantage (from Micro Materials Ltd., Wrexham, UK). The micro-scratch tests with a spheroconical diamond probe of end radius 25 μm were carried out as 3-scan procedures involving a pre-scan surface profile, ramped load scratch and final post-scan surface profile as described in ref. [38]. The critical load data previously shown graphically in [38] are tabulated in Table 1(b). The R_a surface roughness was 11-12 nm on all the coatings.

2.2 Micro-scale reciprocating wear testing

A NanoTest Vantage (Micro Materials Ltd., Wrexham, UK) fitted with a NanoTriboTest module including a reciprocating stage (PI, Germany) controlled within the NanoTest software was used for the reciprocating tests. 500-cycle reciprocating wear tests were performed at 10-500 mN with a diamond indenter of 25 μm end radius as the test probe. In the reciprocating tests the track length was 1 mm and the maximum sliding velocity was 0.5

mm/s. The sliding velocity was at its maximum over the central 90% of the track and linearly reduced to zero at the turn-around points. The total sliding distance was 1 m. For each coating there were 3 repeat tests at 10, 100 and 500 mN, with additional tests at 50 mN and 200 mN on a-C:H, and at 50, 200 and 300 mN on Si-a-C:H. The friction force and the raw (i.e. unlevelled, uncorrected for any instrumental drift or frame compliance contribution) probe displacements were monitored continuously and recorded over the entire wear track. Since the reciprocating stage gradually expands during the tests and no thermal drift correction was applied in this work the on-load depth data were only used to assess changes in roughness/topography as the test proceeded. Final wear widths were determined by confocal microscopy of wear tracks (Keyence VHX-6000). The (dynamic) friction coefficient was determined in software from the energy dissipation during full sliding (Eqn. 1) using an approach similar to that employed by Fouvry and Liskiewicz for friction measurement in fretting tests [41].

μ = Energy dissipation/(2 x track length under full sliding x applied load) Eqn. [1]

The Surface Stress Analyzer (SSA, from SIO, Rugen, Germany) which uses a physical-based analytical methodology to determine simulated stress distributions of the von Mises, tensile and shear stresses during sliding was used to provide simulated stress distributions of the initial sliding contact in the reciprocating tests and in nano-fretting tests at 100 mN with a R = 5 μm probe. Input parameters for the simulations were (i) mechanical properties of the coating (taken as monolayered) and substrate, i.e. hardness (H), elastic modulus (E) and the ratio of hardness to yield stress Y, H/Y (ii) coating thickness (iii) Poisson ratios (iii) probe radius, applied load and measured friction coefficient (taken from previously published micro-scratch test data on these coatings with a diamond indenter of the same nominal

geometry). *H*/*Y* varies strongly with *H*/*E* [42-43]. *H*/*Y* was set to 1.2 for the coatings and 2.5 for the hardened steel substrate.

2.3 Micro-scale impact testing

Micro-impact tests were performed on a NanoTest Vantage system (Micro Materials Ltd., Wrexham, UK) using a spheroconical diamond of end radius 18 μm, as determined by indentation testing on fused silica, as the impact probe. The area function of the probe did not change after the impact tests. The impact energy and effective impact force in an impact test can be controlled by varying the static load and the accelerating distance [44]. In these tests the accelerating distance was set at 40 μm from the initial coating surface and the applied load varied from 500-2000 mN. The load was applied when the indenter is separated from the test surface by the accelerating distance and the load was maintained throughout the impact process. After the probe came to rest it was retracted and the surface re-impacted at the same position, at 4 s intervals. The test duration was 300 s, resulting in 75 impacts in total. For each load there were 5 repeats which were separated by 100 μm. The raw test data are the continuously recorded impact probe position vs. time. A software routine was written to convert these to give the mean depth on coming to rest after each impact. The depth vs. impact cycles data in the figures are under-load, so include the elastic, plastic/fracture deformation. The mean depth data are reported after removing the contribution from the compliance of the test frame.

3. Results

3.1 Micro-scale reciprocating wear

The sensitivity to detect local changes in friction along the scratch track is illustrated by figure 1(a) which shows the raw friction vs. sliding distance data from a test on a-C:H at 500

mN where a change from lower to higher friction occurred rapidly over a few cycles. Figure 1(b) shows friction loops for selected cycles before and after this transition. The slope of the near-vertical section at the beginning and end of the friction loops is the total contact stiffness of the tribosystem, which was ~2000 N/m for the tests at 500 mN. The initial friction coefficient was 0.08-0.10 under all conditions. The evolution in friction coefficient with cycles at 10-500 mN is shown for each of the coatings in figure 2(a-c). At 10 mN the mean friction coefficient averaged over the wear track showed more fluctuations than at higher load for all three coatings. On a-C:H there was a slight decrease with continued cycling at 50-200 mN but at 500 mN there was a transition to higher friction during the tests. Figure 3(a) shows the behaviour in the 3 repeat tests at this load. There was larger variation in the friction over the wear track and in the mean friction per cycle during the test that showed fracture and partial removal than in the other two tests. On Si-a-C:H the friction varied little with continued cycling at 50-200 mN but at ≥300 mN there was a transition to a more periodic friction, although the mean coefficient of friction was unchanged, as illustrated by the three tests at 500 mN in fig. 3(b). On a-C:H:W there was an initial increase in friction at 100 mN to 0.1 before a gradual decrease to $\mu = 0.09$. At 500 mN there was a gradual decrease to a final friction coefficient of ~0.075 (fig. 3 (c)).

SEM images of wear tracks at 500 mN are shown in (figure 4 (a-d)). For a-C:H the wear was relatively low in two of the three tests at 500 mN (one of these is shown in figure 4(a)). However, in the other test on a-C:H there was coating failure over a large part of the track. Figure 4(b) shows a typical transition region between fractured and non-fractured wear track. For the fractured regions EDX revealed Cr and W exposure in the track. The wear depth measured during the test was ~1.5 μm greater in these regions than in the less worn regions. The wear depth monitored during the test showed that with continuing cycles the coating fractured progressively over more of the 1 mm track. There were abrupt changes in apparent

friction on moving between the greater and lesser worn regions. On Si-a-C:H the abrasive marks present in the wear track and debris on the sides of the track were more pronounced (figure 4 (c)). On a-C:H:W the track was smoother with no debris at the sides (figure 4(d)). SEM images (such as in figure 4(a,c and d)) and confocal microscopy showed differences in track width, with a-C:H:W being the widest and a-C:H being narrowest. These differences were present throughout the load range except at 50 mN where track widths were similar on a-C:H and Si:a-C:H and at 10 mN where the Si:a-C:H coating performed best.

3.2 Micro-scale impact testing

Illustrative plots of the variation of impact depth with the number of impacts for tests at 500-2000 mN are shown in Figure 5. On the a-C:H and Si-a-C:H these are characterised by an initial period of rapidly increasing depth over the first few impacts. Thereafter the rate of increase slowed until there was a transition to a more rapid damage rate which gradually slowed, with further transitions between faster and slower damage rates often occurring in the higher load tests. On a-C:H:W after the initial rapid increase in depth as on a-C:H and Si-a-C:H the damage rate continued to decrease through the test so that depth stabilised to reach an approximately constant level after a number of impacts. The transition to a more rapid rate of damage was notably absent on a-C:H:W, although small events were observed occasionally in some of the tests at 1750 and 2000 mN. In these cases the discontinuities in depth that preceded transitions to slightly more rapid damage rates were abrupt small depth reductions (figure 5(f)). The inflexions in the depth data were also absent in 2 of the 5 tests at 500 mN on a-C:H but were seen in every test at ≥750 mN and in all the tests on the Si-a-C:H. SEM and optical imaging showed the inflexions were related to the lateral fracture of the coating system. Lateral fracture was absent in the tests without the inflexions but present in all tests where the inflexions marking the transition to faster damage rate occurred. To more

clearly show how the initial damage evolves across the load range the data from fig. 5(a-b) are replotted as depth increases after the initial impact depth (i.e. setting depth = 0 for the initial impact) for the first 30 impacts in Fig. 5 (d-e). Figs. 5 (d,e) show that the rate of change of probe depth before the inflexion on a-C:H and Si-a-C:H was also load dependent, with the probe depth approaching a plateau only at the lowest loads. The tests showed some variability in the number of impacts required to cause lateral fracture at a given load. The variability for a-C:H was larger than for Si-a-C:H. The load dependence of the mean depth after a single impact, the depth at fracture failure (for a-C:H and Si-a-C:H) and final impact depth are shown in figure 6 (a-c). The figure shows that the probe depth at which failure occurred was dependent on load but was much more consistent from test to test. Final depth comparison is shown in figure 6 (d).

SEM images of selected impact craters are shown for each of the coatings in figures 7-9. Optical imaging confirmed that the tests on a-C:H at 500 mN without the more rapid increases in depth did not show lateral fracture but cracks within the impact crater were observed. There did not appear to be any well-developed radial cracks on a-C:H or Si-a-C:H but extensive lateral cracking was observed (e.g. as in figs. 7,8). In contrast, on a-C:H:W the dominant cracking mechanism was circumferential/radial. From low load there appeared to be a single faint circumferential crack, with ~5-7 μm radial cracks developing from 1000 mN (fig. 9(a)). These gradually increased in number and length at higher loads, with 10-15 μm long cracks observed at 1750-2000 mN (e.g. figure 9(b)). EDX analysis of impact craters on a-C:H showed enhanced Fe, Cr and W at the periphery with C depletion but C remaining in the central region. Similar behaviour was observed on Si-a-C:H (fig. 8). EDX analysis of impact craters on a-C:H:W revealed no compositional changes, including in the two tests at 1750 and 2000 mN where there was lateral cracking between adjacent radial cracks.

4. Discussion

4.1 Influence of coating mechanical properties

The a-C:H, Si-a-C:H and a-C:H:W coatings differed in their mechanical properties and behaviour in the micro-scale reciprocating wear and micro-impact tests, and in previously reported micro-scratch and nano-fretting tests. In particular the behaviour of the softer a-C:H:W was very different to the a-C:H and Si-a-C:H. In addition to being the softest of the three coatings, the a-C:H:W has lower H/E and elastic recovery in indentation than the other coatings. H/E is related to the elastic recovery and elastic and plastic work done in indentation through Eqn. 2:-

$$W_p/(W_p + W_e) \approx 1 - x(H/E_r) \approx h_r/h_{max} \qquad \text{[Eqn. 2]}$$

where W_p is the plastic or irreversible work done during indentation, W_e is elastic deformation, $W_p/(W_p + W_e)$ is a dimensionless plasticity index, h_r is the residual indentation depth and h_{max} is the maximum indentation depth [45]. In low load nanoindentation measurements where substrate contribution is minimised the plasticity index was 0.30 for a-C:H, 0.36 for Si-a-C:H and 0.48 for a-C:H:W. It has been reported that high plasticity index coatings are less susceptible to cracking whilst hard and elastic coatings with lower plasticity can be susceptible to cracking under severe loading as they cannot as easily relieve accumulated strain by plastic flow [13, 38, 39]. In the micro-impact test a-C:H:W showed circumferential and radial cracking but without the significant lateral cracking which occurred from low load on the other coatings. In the micro-scratch test it had higher L_{c1}, L_{c2} and scratch toughness with more localised coating chipping on failure and substrate exposure in the scratch track (i.e. wearing out rather than delamination). However, in reciprocating micro-scale wear tests the a-C:H:W had a lower wear resistance than the other coatings, as it did in reciprocating 4500 cycle nano-fretting tests at 100 mN with a sharper (R = 5 μm)

diamond probe [25]. The relative coating ranking in the 500 cycle reciprocating tests with the R = 25 μm probe is the same as in the reciprocating tests with smaller contact size (nano-fretting tests) but very different to the impact tests with a similar contact size.

4.2 Modelling reciprocating micro-scale wear

In this section analytical modelling of nano- and micro-scratch data has been used to provide an indication of the initial stress state developed in the reciprocating sliding tests. Differences in reciprocating wear behaviour between the coatings can be understood with reference to the stress distribution during initial sliding contact calculated from the probe radii, applied load, friction coefficient and mechanical properties of the indenter, coating and substrate. The simulation results show the regions where the von Mises stresses are greater than the yield stresses so the system is overloaded in these regions and plastic flow is expected. This modelling treatment assumes that the coatings are monolayered, single asperity sphere-on-flat contact and that the surfaces were perfectly smooth, but nevertheless has proved useful in explaining how contact size and coating properties can control the yield location in nano/micro-scale scratch and reciprocating tests. The deformation in nano/micro scratch tests on DLC coatings can be interpreted as effectively single asperity contact with ploughing friction and no/minimal third body wear as the diamond indenters are precision polished to low surface roughness and the DLC surfaces are also smooth (R_a ~0.011 μm).

During sliding contact with a R = 25 μm diamond probe the deformation was initially elastic or very close to it. The 10-500 mN applied loads in the reciprocating tests ranged from well below those resulting in plastic deformation in a single micro-scratch (L_y ~400 mN), to slightly above although the residual depths were ≤50 nm at 500 mN [38]. The maximum von Mises stresses at 500 mN were located within the coatings but analytical modelling showed the location of initial yield was in the substrate due to its lower yield stress. For the lower

yield stress a-C:H:W analytical modelling has shown appreciable yielding within the coating as well (peak von Mises stress in coating at 400 mN was 9.6 GPa) as the substrate. The modelling shows that despite the high stresses developed in the a-C:H and Si-a-C:H coatings they remain below the coating yield stress. The on-load and residual depths in the micro-scratch tests with same nominal probe geometry did not vary noticeably between the three coatings to ≥1500 mN, confirming the role of substrate properties on the initial deformation.

Analytical modelling of the initial stress distribution was also able to explain differences in coating wear in the nano-fretting experiments at 100 mN on these coatings using a sharper diamond probe of 5 μm end radius. At 100 mN the contact was elastic for a-C:H but there was a small region of yield within the coating for Si-a-C:H and more extensive yielded region in the a-C:H:W coating (figure 10). Experimentally, critical load for yield in sliding varied as in Table 2(b). The analytical results are consistent with these differences in the critical load for yield and in on-load and residual depths in scratch and in fretting tests. Although the wear rate was lower on a-C:H fully elastic contact was not observed in reciprocating sliding due to higher contact pressure at asperities on the coating surface. Initial pressures at 500 mN in the reciprocating wear tests were ~14 GPa. The initially very high pressures in the sliding contact were reduced by plastic deformation and wear, with track width measurements from SEM imaging implying the greatest decrease for a-C:H:W (to ~4 GPa) and the least for a-C:H (to ~7 GPa).

Micro-fatigue and cracking

In sliding the shear stress distribution is asymmetric with maximum compressive stress in front of the probe and a maximum tensile stress behind which results in cracking when it exceeds the fracture strength of the coating [46-49]. The load required for cracking (L_{c1}) at the rear of the contact due to high tensile stress of ~5.5-6.3 GPa was ≥1800 mN in the micro-

scratch test, i.e. well above the 10-500 mN in the reciprocating tests [38]. Below the critical load crack formation is possible due to low cycle fatigue. Schiffmann noted that periodic loading in reciprocating sliding leads to an accumulation of plastic deformation and/or densification of the material that gradually increases the subsurface stress in the coating [14,16]. After a number of wear cycles micro-cracks may be formed even though the critical load is not exceeded. Apparent wear at the micro-scale is a combination of material removal and plastic deformation [14,23]. Under these conditions (R = 25 μm, $P \leq 500$ mN) the friction measurements and SEM of wear tracks show that wear of the coatings was dominated by plastic deformation and micro-wear was only a small contributor, particularly for a-C:H:W. The extent of wear is largely controlled by the coatings resistance to plastic deformation (i.e. hardness) rather than fracture resistance. The trends observed between the three coatings parallel those found previously in the nano-fretting tests, where wear correlated with hardness and Y/E [25]. In reciprocating tests with a sharper R = 1 μm diamond Gee et al also reported low wear resistance for a-C:H:W and for other relatively soft coatings (MoST and Graphit-IC from Teer Coatings) in comparison with harder DLC coatings and ceramic coatings [20].

Simple models of abrasive wear, such as Archard's law, focus on hardness as a key parameter although Leyland, Matthews and other authors have shown that H/E (and Y/E) may be more reliable [50-52]. In these micro-wear tests an additional consideration for coatings is that the wear is influenced by the yield position and the size of the contact can therefore be critical. Michler and Blank have shown that the ratio of indenter radius to coating thickness is important in determining where cracking begins in indentation contact [53]. In a repetitive sliding contact the applied load is another important factor since this influences the depth of the peak von Mises stresses. To illustrate this, Shi and co-workers showed how the relative performance of a-C coatings in repetitive scratch tests varied with applied load and hence peak stress position [13]. Under light loading peak stresses were within the coating and

coatings with highest hardness performed best but at higher load peak stresses were localised at the interface and fracture was more important, resulting in an inversion in performance with lower hardness coatings (with hardness more closely matched to substrate) performing much better.

Friction in micro-scale reciprocating wear

Although friction loops revealed the presence of occasional track-position sensitive changes in friction, determining an average friction coefficient from the energy dissipation over the entire track sliding at full velocity proved a reliable approach enabling differences between coatings as a function of load and cycles to be investigated. The friction coefficient at the start of the reciprocating tests was ~0.08-0.10, which was close to that determined in (non-reciprocating) micro-scratch tests with a probe of the same nominal geometry, as illustrated in Table 2(c) for 100 and 500 mN. In the reciprocating tests at 10 mN the friction coefficient shows more fluctuations between cycles than at higher loads. Achanta and co-workers also reported higher variability in friction in smaller scale contact [15,17,19]. They considered that the surface topography influences the frictional fluctuations through two major effects, geometrical (local slope/ratchet mechanism) and adhesive (contact area). In the current study the slight increase in friction observed during the first ~50 cycles for all three coatings before levelling out is considered to be a surface topographical effect through increasing contact area and the difficulty in forming a transfer layer in light multi-asperity contact on rough surfaces [54].

Running-in effects causing changes in friction during the first few cycles at >10 mN are related to increasing contact area as asperities break down. When there is high surface conformity and the average gap between the surfaces is very low adhesion dominates friction, so friction scales with contact area [55]. Increasing friction during the fretting testing of a

hard DLC coating against a Si_3N_4 ball under gross slip conditions (100 mN, R = 2.5 mm, displacement amplitude = 300 μm, 0.2 Hz) has been interpreted as changing roughness and break-down of asperities on both surfaces, with a limiting value associated with a reduction in average asperity inclination in multi-asperity contact [17]. The subsequent constant friction was explained as third body wear with micro-particles rolling in the contact. The grooving wear appearance of the wear track at 500 mN on Si-a-C:H is consistent with this interpretation. There is minimal ploughing and smoothening of the wear track that would result in friction reduction.

As the load was increased the influence of the local surface topography in the wear track on the mean friction coefficient decreased. The main exception to this was the 500 mN test on a-C:H where fracture occurred accompanied by spikes in friction. To a lesser extent the friction force was also more variable in the other tests at 500 mN after the transition (see figure 3(a)). The micro-cracking in these tests may be the start of the low cycle fatigue process that is sensitive to areas of coating inhomogeneity. Santner and co-workers have described geometric changes in friction where sliding probes encounter topographic features [56-59]. These authors observed sharp increases in friction sliding up steps and similar reduction sliding down steps. Adhesion was ruled out as the explanation since the effect was present in oil and in air [57], although triboreaction layers and wear particles could obscure the topographical effects [59].

In the tests at 100-500 mN on a-C:H:W and 50-200 mN on a-C:H the friction continued to decrease with further wear cycles after the running-in stage. On a-C:H:W the SEM image (fig. 4) shows a very smooth wear track at 500 mN with no debris at the edges consistent with a reduction in the ploughing component to the measured friction. As shown by Korres et al [60], when there is minimal third body wear there is a correlation between track widening and

a reduction in the ploughing component to friction. The a-C:H:W coating is reported to have a microlamellar structure with alternating C- and WC-rich layers (produced by rotation during deposition) which may shear easily, and provide low friction [40], consistent with the smooth appearance of the wear track (and wear tracks in nano- and micro-scale scratch testing).

Reciprocating vs. unidirectional sliding

In low-cycle repetitive scratch testing of amorphous carbon films the friction initially reduces due to the ploughing contribution decreasing then, provided there is no adhesive failure, stabilises within a few cycles at μ~0.08 [61]. On a-C:H the more pronounced decrease with cycling at 50-200 mN to reach values of 0.04-0.08 may be related to formation of a low-friction graphitic tribolayer. Holmberg and co-workers also noted decreasing friction to reach μ~0.04-0.06 in reciprocating sliding on DLC-DLC contacts, with a greater reduction in friction than in pin-on-disk tests [54]. In a study of unrepeated and repeated reciprocating sliding, where each cycle was on a virgin region of the surface in the unrepeated sliding tests, it was reported that repeated sliding promotes the formation of a third body composed of compressed wear particles that stabilizes the friction [55]. Singer and co-workers showed that a low friction, partially graphitised tribolayer can form in sliding on DLC [62], as has been reported elsewhere, e.g. in boundary lubricated sliding of an a-C:H coating produced with the same multilayer structure, against steel [63]. This friction reduction mechanism does not appear to be effective at 500 mN. The abrupt increases soon after the start of the test may be related to micro-cracking resulting in more topographical influence on friction. Initially increasing friction before levelling out has also been observed on a-C:H in nano-fretting tests [25]. On Si-a-C:H the mean friction is constant from 50-500 mN, although at ≥300 mN

periodic changes suggestive of some micro-cracking were noted, which are consistent with the SEM image showing abrasive/grooving wear.

Extent of friction-wear correlation

The dissipated energy during reciprocating sliding contacts has been used as a measure of wear rate, based on the assumption that the majority of the frictional losses occur through plastic deformation and cracking [64-65]. This approach has mixed success with micro-scale reciprocating contacts. In nano-fretting tests [25] the friction increases more rapidly with cycles on a-C:H:W which showed much higher wear rate than the other two coatings. Friction forces in nano-fretting experiments were higher than in the reciprocating tests, particularly on a-C:H:W. The higher values reflect the dominant contribution of changing attack angle when wearing to greater depth for the sharper probe [66,67]. However, a friction-wear correlation was less clear in the micro-scale single-asperity contacts at 500 mN (since the highest wear is for a-C:H:W which has the lowest friction). In 25-cycle reciprocating tests with a R = 1 μm diamond Gee et al also reported that the micro-scale friction coefficient was μ = 0.04-0.08 for a range of soft and hard coatings and there was no particular correlation to either macro-scale friction or to micro-scale wear [20]. The authors speculated whether capillary forces were responsible, with water from the moist atmosphere in which the tests were performed forming a lubricating layer between indenter and sample exerting a large influence on the friction at the micro-scale. The similarities in the friction evolution in these contacts with 1, 5 and 25 μm radius diamond probes which can be largely understood in terms of the varying contributions of ploughing, changing contact area and micro-wear.

4.3 Impact

In contrast to its poor wear resistance in reciprocating sliding, the a-C:H:W coating displayed much better performance than the other coatings when subjected to repetitive impact. Despite differences in the contact conditions in micro-scale scratch and impact tests in both of these tests a-C:H:W was the most crack resistant coating and Si-a-C:H least crack resistant. Although it has been stated that Si-doping can improve DLC adhesion this was not the case for the current coatings. The adverse effect of Si-doping on wear resistance was in agreement with other findings in the literature (summarised in ref 37). Differences in impact and scratch resistance with the mechanical properties of carbon coatings have also been observed for graded C/Cr and graded a-C:H coatings on M42 steel under similar conditions [39]. With relatively low hardness (14 GPa), high plasticity (H/E = 0.077) and low resistance to plastic deformation (H^3/E^2 = 0.82 GPa) the C/Cr coating has mechanical properties similar to a-C:H:W and also exhibited good performance in the micro-scratch and impact tests, with more localised rather than extensive cracking in micro-scratch tests and no lateral cracking in micro-impact tests.

Substrate load carrying capacity has an important role on the behaviour of the coating system. All the DLC coatings underwent dramatic impact failure when deposited on unhardened tool steels or stainless steel, substrates with much lower load carrying capacity, even at lower load [68]. Poor fatigue resistance of the a-C:H and Si-a-C:H coatings on hardened tool steel under repetitive micro-impact contrasts with TiAlN-based nitride coatings on cemented carbide where increased H^3/E^2 in the nitride coating or the carbide substrate improved their fatigue resistance in the micro-impact test [69-71]. The carbon coatings were deposited on a substrate with lower hardness and elastic modulus than cemented carbide. The steel substrate provides less load support, and the resulting increased substrate deformation causes the coatings to be subjected to higher bending strains at a given load. For this reason a-C:H and Si-a-C:H coatings on hardened tool steels impact resistance is not improved by increasing

coating hardness and H^3/E^2. The smaller difference in hardness between the coating and the hardened tool steel substrate in a-C:H:W and C/Cr helps the coating to accommodate plastic deformation of the substrate without cracking [72]. In a study of nitrogen-containing chromium ($Cr_{1-x}N_x$) coatings on a softer stainless steel Rebholz and co-workers noted that the hardest coating with Cr_2N cracked most in impact testing but the impact crater volume was low [73]. In contrast, coatings with x =0.10-0.16, where the nitrogen is incorporated in solid solution, were softer (H ~10-14 GPa) and more ductile with only small amounts of radial cracking in impact and higher L_{c2} in scratch tests.

Deformation in the micro-impact test was strongly load dependent since the extent of plastic and elastic deformation of the steel substrate, and hence coating bending and tensile stresses developing at the edge of the contact is controlled by the applied load. Increasing the applied load resulted in greater substrate deformation and higher tensile stresses and failure became more severe and occurred after fewer impacts on a-C:H and Si-a-C:H. In simulated stress distributions by analytical modelling of micro-scratch tests the a-C:H:W coating can tolerate a higher tensile stress than the other coatings [74].

The ratio between coating thickness t and indenter radius R (t/R) in the micro-impact tests was 0.17-0.22. A FEA study of spherical indentation of DLC on a tool steel substrate with Y = 2 GPa showed that this ratio influences the failure behaviour [53]. In this coating system the initial damage was by substrate plasticity at, or below, the coating-substrate interface. The subsequent preferred location for cracks to nucleate was determined by the position of peaks in the principal stress. For t/R = 0.33 crack nucleation at the interface was dominant although circumferential cracks also nucleate at the surface at radial distances up to twice the contact radius. For t/R = 0.033 interfacial and circumferential cracking were predicted.

Experimental studies have shown the importance of substrate stiffness and load support in cracking in indentation and scratch tests [75-77]. From FIB x-sections of scratch tracks on DLC on stainless steel Xie and co-workers noted that lateral cracking was the result of intersection of cracks originating at the interface and the surface [75]. Borrero-López and co-workers found that a more compliant and soft substrate promoted cracking at the DLC coating surface but a more stiff and hard substrate resulted in median and lateral cracking [76]. Wang and co-workers noted that increasing substrate hardness generated higher stresses in the substrate which reduced the interface strain, delaying fracture until higher contact load [78].

As mentioned above, when deposited on unhardened tool steel or stainless steel substrates that both have much lower load carrying capacity, the un-doped, Si-doped and W-doped coatings cracked on immediate impact. However, the coatings studied here were deposited on a hardened steel substrate, and in the case of a-C:H:W, with a hard CrN sub-layer, that provides improved load support so their mechanical properties do not decrease as dramatically as the indentation depth increases as with a soft and compliant substrate. This was confirmed by nanoindentation tests to ~25-30% of the total coating thickness that revealed little change in hardness from tests at much lower depth. Although the hardened substrate improved impact resistance somewhat, there was cracking after a few impacts on a-C:H and Si-a-C:H. The SEM images in figures 7-8 show delamination, consistent with cracking starting at or near the interfaces, as was observed in the studies above, in FIB sections of impact craters on Si-a-C:H [79] and on graded a-C:H under similar test conditions [39].

On a-C:H:W there was radial cracking but interfacial cracking was completely absent. McMaster and co-workers reported FIB-images of impact cross-sections (R~13.5 μm, 1 N) to

show that there was cohesive cracking for a-C:H:W deposited without a CrN sublayer but again interfacial delamination was not observed [79]. Ramirez and co-workers reported enhanced resistance to contact fatigue for W-doped DLC with ~7.5 GPa hardness on hardened tool steel [35]. In comparison to TiN-coated steel which fractured under the same conditions, they found cohesive and adhesive damage was suppressed in the W-doped coating. In cyclic loading of brittle ceramics with spherical tungsten carbide indenters radial cracks were observed that were absent in single loading [33]. In cyclic Vickers indentation of hard coatings on tool steels the type of cracking depended on the H/E ratio of the coatings [80]. A quasi-plastic damage mode with radial cracks that grew with number of cycles was typical in lower H/E coatings. Karimi and co-workers reported that radial cracking was more common in Berkovich and Vickers indentation than in spherical indentation [81]. In TiAlSiN coatings they noted that radial crack propagation was favoured by (i) nanolayer structure (ii) small elastic modulus mismatch (iii) good adhesion and (iv) high toughness of the coating and substrate. Despite being much softer, when deposited on hardened steel the a-C:H:W coating appears to have similar beneficial properties.

The micro-impact tests at higher load allow the increasing contribution of the substrate to the composite response to be studied whilst retaining sensitivity to the coating properties. Figure 11 shows how the mean damage rate over the final 10 impacts varied with load. The rate is highest for Si-a-C:H throughout the load range and lowest on a-C:H:W. This difference reflects whether fracture has occurred and subsequent damage tolerance of the system. The error bar on a-C:H:W remains small until 1750 mN when some of the tests show some small depth depths associated with cohesive lateral cracking that cause stress rearrangements under the probe (see figs. 5(f) and 9(b)). The gradual increase in depth of ~ 2-3 nm/impact on a-C:H:W at these loads was slightly higher than the ~1 nm/impact at lower load and ~1 nm/impact for graded C/Cr on hardened M42 tool steel where the small depth decreases and

cohesive fractures were not observed under the same experimental conditions. The gradual ~1 nm/impact increase in depth may be a combination of coating wear with some substrate fatigue involving fracture of carbides in the steel substrate. In studies of contact fatigue of coated tool steels Ramirez and co-workers showed sensitivity to the steel microstructure, with large primary carbides acting as stress concentrators [82].

5. Conclusions and outlook

The capability for high cycle, high speed, long sliding distance reciprocating sliding at the mN level has been incorporated into commercial nanomechanical test instrumentation, where the high lateral rigidity of the loading head is retained together with sensitive friction and depth measurement. This capability could provide a linkage across the length scales usually probed in nano- or macro- scale tribological tests and enable the study of running-in processes in greater detail than possible previously. Although a diamond probe with 25 μm end radius was used in the reciprocating tests to provide direct comparison with micro-scratch tests on these samples, larger radius probes could be used and longer wear tests run in future work. Since electrical contact resistance monitoring has been shown to be a valuable tool for detecting premature wear of DLC sliding against steel in a pin-on-disk test by dielectric breakdown [83] this approach could be used for the micro-scale reciprocating tests, using an electrically conductive boron-doped diamond probe.

Analytical modelling of nano- and micro-scratch data provided an indication of the initial stress state developed in the reciprocating sliding tests which could explain differences in reciprocating wear resistance. Under the test conditions the deformation in the wear track was largely controlled by plastic deformation and hence hardness since micro-scale fatigue wear was only a small contributor. Si- and W-doped DLC coatings, which are softer than the undoped DLC therefore showed lower wear resistance in reciprocating sliding.

Micro-scale repetitive impact tests revealed differences between the coatings which correlated to their behaviour in micro-scratch tests. There was low resistance to impact-induced fracture and more extensive cracking in the scratch tests for a-C:H and Si-a-C:H. Whilst high H/E and H^3/E^2 can be advantageous in impact tests of coatings on cemented carbide the same trends were not observed on the tool steel. The hard and elastic undoped and Si-doped DLC coatings perform poorly due to a combination of factors: (i) lower load support from the softer and lower modulus tool steel increasing bending stresses in the coating (ii) being amorphous they have limited micro-toughening mechanisms (iii) low plasticity (iv) lower interfacial strength. In contrast the W-doped DLC exhibited excellent impact resistance. This coating has (i) lower hardness and H/E (ii) closer hardness to substrate (iii) lamellar structure.

In reciprocating sliding the coating ranking changed, with the hardest coating showing the highest wear resistance. The results emphasize the importance of considering contact conditions in coating choice as the optimum mechanical properties (balance of load support and fracture resistance) vary with the test. The relative performance of the three coatings was dependent on the type and severity of the test and the contact length scale as controlled by the applied load and test probe radius. Table 3 summarises the relative coating ranking in the different nano/microtribological tests. In terms of hardness, H/E and H^3/E^2, the coatings rank as a-C:H > Si-a-C:H > a-C:H:W, which is beneficial in situations where load support is more critical than fracture resistance. The length-scale probed by the test is also important. Micro-impact correlates with micro-scratch as both tests probe the complete coating-substrate system whereas the reciprocating micro-scale wear test correlates with nano-fretting and the onset of yield in nano-scratch as the stresses are concentrated in the coating. The friction coefficients of the coatings vary with the contribution of ploughing friction in the different tribological tests. A benefit of the micro-impact test lies in its ability to concentrate stresses

near the interfaces in coating systems. At higher load it can be used to study the increasing contribution of the substrate to the composite response whilst retaining high sensitivity to the coating properties.

Acknowledgements

This work was supported by the Engineering and Physical Sciences Research Council (EPSRC), Grant No. ELP01629X and Micro Materials Ltd. as part of the EPSRC Doctoral Training Centre in Integrated Tribology (iT-CDT). Prof. Vladimir Vishnyakov (University of Huddersfield, UK) is thanked for useful discussions and Hayley Andrews (Manchester Metropolitan University) is acknowledged for the SEM imaging of the wear tracks.

References

1. J.A. Greenwood and J.P. Williamson, Contact of nominally flat surfaces, Proc. Royal Soc. London A 295 (1966) 300-319.
2. T.R. Thomas, Roughness and function, Surf. Topogr.: Metrol. Prop. 2 (2014) 014001 (10pp).
3. B. Bhushan, Contact mechanics of rough surfaces in tribology: single asperity contact, Appl. Mech. Rev. 49 (1996) 275-298.
4. W.G. Sawyer and K.J. Wahl, Accessing Inaccessible Interfaces: In Situ Approaches to Materials Tribology, MRS Bull. 33 (2008) 1145-1150.
5. P. Stoyanov, R.R. Chromik, Scaling Effects on Materials Tribology: From Macro to Micro Scale, Materials 10 (2017) 550 (49pp).
6. J.H. Dieterich, B.D. Kilgore, Direct observation of frictional contacts: new insights for state-dependent properties, Pure and Applied Geophysics 143 (1994) 283-302.

7. T.D.B. Jacobs, C. Greiner, K.J. Wahl, R.W. Carpick, Insights into tribology from in situ nanoscale experiments, MRS Bull. 44 (2019) 478-486.
8. I. Szlufarska, M. Chandross and R.W. Carpick, Recent advances in single-asperity nanotribology, J. Phys. D: Appl. Phys. 41 (2008) 123001 (39pp).
9. K. Degiampietro, R. Colaço, Nanoabrasive wear induced by an AFM diamond tip on stainless steel, Wear 263 (2007) 1579-1584.
10. Z.-D. Sha, V. Sorkin, P.S. Branicio, Q.-X. Pei, Y.-W. Zhang and D.J. Srolovitz, Large-scale molecular dynamics simulations of wear in diamond-like carbon at the nanoscale, Appl. Phys. Lett. 103 (2013) 073118.
11. R. Aghababaei, T, Brink, and J.-F. Molinari, Asperity-Level Origins of Transition from Mild to Severe Wear, Phys. Rev. Lett. 120 (2018) 186105.
12. Y. Liao, L. Marks, In situ single asperity wear at the nanometre scale, Int. Mater. Rev. (2016) 1-17. DOI 10.1080/09506608.2016.1213942.
13. B. Shi, J.L. Sullivan and B.D. Beake, An investigation into which factors control the nanotribological behaviour of thin sputtered carbon films, J Phys D: Appl Phys 41 (2008) 045303.
14. K.I. Schiffmann, A. Hieke, Analysis of microwear experiments on thin DLC coatings: friction, wear and plastic deformation, Wear 254 (2003) 565–572.
15. D. Drees, J.-P. Celis, S. Achanta, Friction of thin coatings on three length scales under reciprocating sliding, Surf. Coat. Technol. 188-189 (2004) 511-518.
16. K.I. Schiffmann, Phenomena in microwear experiments on metal-free and metal-containing diamond-like carbon coatings: friction, wear, fatigue and plastic deformation, Surface and Coatings Technology 177 –178 (2004) 453–458.
17. S. Achanta, D. Drees, J.-P. Celis, Friction and nanowear of hard coatings in reciprocating sliding at milli-Newton loads, Wear 259 (2005) 719-729.

18. M.G. Gee, A.D. Gee, A cost effective system for micro-tribology experiments, Wear 263 (2007) 1484-1491.
19. S. Achanta, D. Drees, J.-P. Celis, Friction from nano to macroforce scales analysed by single and multiple-asperity contact approaches, Surf. Coat. Technol. 202 (2008) 6127-6135.
20. M. G. Gee, J.W. Nunn, A. Muniz-Piniella, L.P. Orkney, Micro-tribology experiments on engineering coatings, Wear 271 (2011) 2673-2680.
21. G.M. Wilson, J.F. Smith, J.L. Sullivan, A nanotribological study of thin amorphous C and Cr doped amorphous C coatings, Wear 265 (2008) 1633-1641.
22. G.M. Wilson, An investigation of thin amorphous carbon-based sputtered coatings for MEMS and Micro-engineering applications, PhD Thesis, Aston University, 2008.
23. P. Stoyanov, R.R. Chromik, S. Gupta, J.R. Lince, Micro-scale sliding contacts on Au and Au-MoS_2 coatings, Surf. Coat. Technol. 205 (2010) 1449-1454.
24. P. Stoyanov, S. Gupta, R.R. Chromik, J.R. Lince, Microtribological performance of Au–MoS_2 nanocomposite and Au/MoS_2 bilayer coatings, Tribol. Int. 52 (2012) 144-152.
25. T.W. Liskiewicz, B.D. Beake, N. Schwarzer and M.I. Davies, Short note on improved integration of mechanical testing in predictive wear models, Surf. Coat. Technol. 237 (2013) 212.
26. B.D. Beake, A.J. Harris, T.W. Liskiewicz, J. Wagner, S.J. McMaster, S.R. Goodes, A. Neville and L. Zhang (accepted for publication in Wear, March 2021).
27. J.A. Williams, H.R. Le, Tribology and MEMS, J.Phys.D: Appl.Phys. 39 (2006) R201–R214.
28. R. Gåhlin, M. Larsson, P. Hedenqvist, Me-C:H coatings in motor vehicles, Wear 249 (2001) 302-309.

29. S.D.A. Lawes, S.V. Hainsworth, M.E. Fitzpatrick, Impact wear testing of diamond-like carbon films for engine valve-tappet surfaces, Wear 268 (2010) 1303-1308.
30. K. Holmberg, P. Andersson, A. Erdemir, Global energy consumption due to friction in passenger cars, Tribol. Int. 147 (2012) 221-234.
31. K. Holmberg, A. Erdemir, Influence of tribology on global energy consumption, costs and emissions, Friction 5 (2017) 263–284.
32. M. Woydt, R. Luther, T. Gradt, A. Rienäcker, T. Hosenfeldt, F.-J. Wetzel and C. Wincierz, Tribology in Germany; Interdisciplinary technology for the reduction of CO2-emissions and the conservation of resources, pp1-34, 2019, Gesellschaft für Tribologie e.V. (German Society for Tribology e.V. www.gft-ev.de) Jülich, Germany.
33. D.K. Kim, Y.-G. Jung, I.M. Peterson, B.R. Lawn, Cyclic fatigue of intrinsically brittle ceramics in contact with spheres, Acta Mater. 47 (1999) 4711-4725.
34. G. Ramírez, E. Tarres, B. Casas, I. Valls, R. Martinez, L. Llanes, Contact fatigue behaviour of PVD-coated steel, Plasma Process Polym. 6 (2009) S588–91.
35. G. Ramírez, E. Jiménez-Piqué, A. Mestra, M. Vilaseca, D. Casellas, L. Llanes, A comparative study of the contact fatigue behaviour and associated damage micromechanisms of TiN- and WC:H- coated cold-work tool steel, Tribol. Int. 88 (2015) 263-270.
36. O. Wänstrand, M. Larsson, P. Hedenqvist, Mechanical and tribological evaluation of PVD WC/C coatings, Surface and Coatings Technology 111 (1999) 247–254.
37. J.L. Lanigan, C. Wang, A. Morina, A. Neville, Repressing oxidative wear within Si doped DLCs, Tribol. Int. (2016).
38. B.D. Beake, T.W. Liskiewicz, V.M. Vishnyakov and M.I. Davies, Development of DLC coating architectures for demanding functional surface applications through nano- and micro-mechanical testing, Surf. Coat. Technol. 284 (2015) 334-343.

39. B.D. Beake, T.W. Liskiewicz, A. Bird, X. Shi, Micro-scale impact testing - A new approach to studying fatigue resistance in hard carbon coatings, Tribol. Int., 149 (2020) 105732 (10pp).
40. Coated components: greater performance and reliability, Oerliken Balzers Technical Note, 3rd Edition 2010.
41. T. Liskiewicz, S. Fouvry, Development of a friction energy capacity approach to predict the surface coating endurance under complex oscillating sliding conditions, Tribol. Int. 38 (2005) 69-79.
42. L.J. Vandeperre, W. J. Clegg, The Correlation between Hardness and Yield Strength of Hard Materials, Functionally Graded Materials VIII, Materials Science Forum 492-493 (2005) 555-560.
43. A. Clausner, F. Richter, Determination of yield stress from nano-indentation experiments, Eur. J. Mech. A Solid 51 (2015) 11-20.
44. C. Zehnder, J.-N. Peltzer, J.S.K.-L. Gibson, S. Korte-Kerzel, High strain rate testing at the nano-scale: a proposed metholodogy for impact nanoindentation, Mater. Design. 151 (2018) 17-28.
45. Y.-T. Cheng and C.-M. Cheng, Scaling, dimensional analysis, and indentation measurements, Mater. Sci. Eng. R 44 (2004) 91-149.
46. G.M. Hamilton and L. E. Goodman, The Stress Field Created by a Circular Sliding Contact, J. Appl. Mech., 33 (1966) 371.
47. T. Chudoba, N. Schwarzer and F. Richter, Steps towards a mechanical modelling of layered systems. Surf. Coat. Technol. 154 (2002) 140.
48. K. Holmberg, H. Ronkainen, A. Laukkanen and K. Wallin, Friction and wear of coated surfaces – scales, modelling and tribomechanisms, Surf. Coat. Technol. 202 (2007) 1034-1049.

49. K. Holmberg, H. Ronkainen, A. Laukkanen and K. Wallin, A. Erdemir and O. Eryilmaz, Tribological analysis of TiN and DLC coated contacts by 3D FEM modelling and stress simulation, Wear 264 (2008) 877-884.
50. A. Leyland and A. Matthews, Design criteria for wear-resistant nanostructured glassy-metal coatings, Surf. Coat. Technol. 177-178 (2004) 317-324.
51. A. Leyland and A. Matthews, On the significance of the H/E ratio in wear control: a nanocomposite coating approach to optimised tribological behaviour, Wear 246 (2000) 1-11.
52. W. Ni, Y.-T. Cheng, M.J. Lukitsch, A.M. Weiner, L.C. Lev, D.S. Grummon, Effects of the ratio of hardness to Young's modulus on the friction and wear behavior of bilayer coatings, Appl. Phys. Lett. 85 (2004) 4028-4030.
53. J. Michler, E. Blank, Analysis of coating fracture and substrate plasticity induced by spherical indentors: diamond and diamond-like carbon layers on steel substrates, Thin Solid Films 381 (2001) 119-134.
54. K. Holmberg, A. Laukkanen, H. Ronkainen, R. Waudby, G. Stachowiak, M. Wolski et al, Topographical orientation effects on friction and wear in sliding DLC and steel contacts, part 1: Experimental, Wear 330-331 (2015) 3-22.
55. F.-C. Hsia, F.M. Elam, D. Bonn, B. Weber, S.E. Franklin, Wear particle dynamics drive the difference between repeated and non-repeated reciprocated sliding, Tribol. Int. 142 (2020) 105983.
56. E. Santner, D. Klaffke, K. Meine, C. Polaczyk, D. Spaltmann, Demonstration of topography modification by friction processes and vice versa, Tribol. Int. 39 (2006) 450-455.
57. K. Meine, T. Schneider, D. Spaltmann, E. Santner, The influence of roughness on friction Part I. The influence of a single step, Wear 253 (2002) 725-732.

58. K. Meine, T. Schneider, D. Spaltmann, E. Santner, The influence of roughness on friction Part II. The influence of multiple steps, Wear 253 (2002) 733-738.
59. E. Santner, D. Klaffke, K. Meine, C. Polaczyk, D. Spaltmann, Effects of friction on topography and vice versa, Wear 261 (2006) 101-106.
60. S. Korres, T. Feser, M. Dienwiebel, A new approach to link the friction coefficient with topography measurements during plowing, Wear 303 (2013) 202-210.
61. NANOINDENT-PLUS 'Standardising the nano-scratch test' EU FP7 project NMP-2012-CSA-6-319208.
62. I. L. Singer, S. D. Dvorak, K. J. Wahl, and T. W. Scharf, Role of third bodies in friction and wear of protective coatings, J. Vac. Sci. Technol. A 21 (2003) S232-S240.
63. Papken Eh. Hovsepian, P. Mandal, Arutiun P. Ehiasarian, G. Sáfrán, R. Tietema, D. Doerwald, Friction and wear behaviour of Mo-W doped carbon-based coating during boundary lubricated sliding. Appl. Surf. Sci. 366 (2016) 260-274.
64. M.Z. Huq, J.-P. Celis, Expressing wear rate in sliding contacts based on dissipated energy, Wear 252 (2002) 375–383.
65. T. Liskiewicz, S. Fouvry, Development of a friction energy capacity approach to predict the surface coating endurance under complex oscillating sliding conditions, Tribol. Int. 38 (2005) 69-79.
66. K.I. Schiffmann, Microtribological/mechanical testing in 0, 1 and 2 dimensions: A comparative study on different materials, Wear 265 (2008) 1826-1836.
67. S. Lafaye, M. Troyon, On the friction behaviour in nanoscratch testing, Wear 261 (2006) 905-913.
68. S.J. McMaster, unpublished.

69. B.D. Beake, L. Isern, J.L. Endrino, G.S. Fox-Rabinovich, Micro-impact testing of AlTiN and TiAlCrN coatings, Wear 418-419 (2019) 102-110.
70. B.D. Beake, A. Bird, L. Isern, J.L. Endrino, F. Jiang, Elevated temperature micro-impact testing of TiAlSiN coatings produced by physical vapour deposition, Thin Solid Films 688 (2019) 137358 (9pp).
71. N. Cinca, B.D. Beake, A.J. Harris, E. Tarrés, Micro-scale impact testing on cemented carbide, Int. J. Refract. Met. Hard Mater. 84 (2019) 105045 (9pp).
72. E. Bousser, M. Benkahoul, L. Martinu and J.E. Klemberg-Sapieha, Effect of microstructure on the erosion resistance of Cr-Si-N coatings, Surf. Coat. Technol. 203 (2008) 776-780.
73. C. Rebholz, H. Ziegele, A. Leyland, A. Matthews, Structure, mechanical and tribological properties of nitrogen-containing chromium coatings prepared by reactive magnetron sputtering, Surf. Coat. Technol. 115 (1999) 222-229.
74. B.D. Beake, T.W. Liskiewicz, V.M. Vishnyakov, presented at 44th ICMCTF, San Diego, 24-28 April, 2017.
75. Z.-H. Xie, R. Singh, A. Bendavid, P.J. Martin, P.R. Munroe, M. Hoffman, Contact damage evolution in a diamond-like carbon (DLC) coating on a stainless steel substrate, Thin Solid Films 515 (2007) 3196-3201.
76. O. Borrero-López, M. Hoffman, A. Bendavid, P.J. Martin, Substrate effects on the mechanical properties and contact damage of diamond-like carbon films, Diam. Relat. Mater. 19 (2010) 1273-1280.
77. S. Sveen, J.M. Andersson, R.M'Saoubi, M. Olsson, Scratch adhesion characteristics of PVD TiAlN deposited on high speed steel, cemented carbide and PCBN substrates, Wear 308 (2013) 133-141.

78. C.T. Wang, T.J. Hakala, A. Laukkanen, H. Ronkainen, K. Holmberg, N. Gao et al, An investigation into the effect of substrate on the load-bearing capacity of thin hard coatings, J. Mater. Sci. 51 (2016) 4390-4398.
79. S.J. McMaster, T.W. Liskiewicz, A. Neville, B.D. Beake, Probing fatigue resistance in multi-layer DLC coatings by micro- and nano-impact: Correlation to erosion tests, Surf. Coat. Tech. (2020) 126319.
80. A. Sivitski, A. Gregor, M. Saarna, P. Kulu, F. Sergejev, Estonian J. Eng. 15 (2009) 309-317. doi:10.3176/end.2009.4.08.
81. A. Karimi, Y. Wang, T. Cselle, M. Morstein, Fracture mechanisms in nanoscale layered hard thin films, Thin Solid Films 420-421 (2002) 275–280.
82. G. Ramírez, A. Mestra, B. Casas, I. Valls, R. Martínez, R. Bueno, A. Góez, A. Mateo, L. Llanes, Influence of substrate microstructure on the contact fatigue strength of coated cold-work tool steels, Surf. Coat. Technol. 206 (2012) 3069-3081.
83. F.G. Echeverrigaray, S.R.S de Mello, L.M. Leidens, C.D. Boeira, A.F. Michels, I. Braceras, C.A. Figueroa, Electrical contact resistance and tribological behaviors of self-lubricated dielectric coating under different conditions, Tribol. Int. 143 (2020) 106086.

Tables

Table 1 (a) Typical test conditions in nano- and microtribological tests

	AFM wear	Repetitive nano-scratch	Nano-fretting	NanoTriboTest
Motion	Reciprocating	Unidirectional	Reciprocating	Reciprocating
Sliding speed (mm/s)	0.001-0.25	0.001-0.1	0.01	1-10
Track length (mm)	0.001-0.1	0.01-1	0.02	1-10
Number of cycles	1-50	1-20	1000-200000	100-30000
Total sliding distance (m)	0.000001-0.001	0.00001-0.01	0.01-0.1	0.1-300
Probe radius (μm)	0.02-1	5-25	10-200	25-5000

Table 1 (b) Comparison of tribological test conditions

	Nano-fretting	Nano-scratch	Micro-scratch	Reciprocating micro-wear	Micro-impact
Probe Radius (μm)	5	5	25	25	20
Applied Load (mN)	100	Ramped to 500	Ramped to 5000	10-500	500-2000
Cycles under load	4500	1	1	500	75
Reference	[25]	[38]	[38]	This work	This work

Table 2 (a) Coating structure and mechanical properties

Short name	Coating structure	*H* (GPa)	*E* (GPa)	*H/E*	H^3/E^2 (GPa)
a-C:H	0.3 μm Cr/0.7 μm W-C:H/2.9 μm a-C:H	23.4 ± 1.2	226 ± 13	0.104	0.254
Si-a-C:H	0.3 μm Cr/0.7 μm W-C:H/2.8 μm Si-a-C:H	16.2 ± 0.6	157 ± 4	0.103	0.173
a-C:H:W	1 μm CrN/2 μm a-C:H:W	11.5 ± 0.9	161 ± 7	0.072	0.059

From nanoindentation at 20 mN. Contact depths were 4-8 % of the total coating thickness.

Table 2 (b) nano- and micro-scratch critical loads

Coating	*R* = 5 μm nano-scratch			*R* = 25 μm micro-scratch		
	L_y (mN)	L_{c1} (mN)	L_{c2} (mN)	L_y (mN)	L_{c1} (mN)	L_{c2} (mN)
a-C:H	206 ± 5	422 ± 4	> 500	356 ± 9	2179 ± 120	2612 ± 127
Si-a-C:H	110 ± 10	445 ± 12	> 500	383 ± 52	1827 ± 111	2830 ± 367
a-C:H:W	68 ± 4	>500	> 500	375 ± 49	2256 ± 116	3695 ± 132

Peak load 500 mN in nano-scratch; 5000 mN in micro-scratch.

Table 2 (c) Micro-scratch friction coefficient

	μ at 100 mN	μ at 500 mN
a-C:H	0.067 ± 0.015	0.077 ± 0.013
Si-a-C:H	0.084 ± 0.021	0.082 ± 0.003
a-C:H:W	0.079 ± 0.015	0.108 ± 0.003

R = 25 μm diamond.

Table 3 Relative coating behaviour in different tribological tests

	Nano-fretting	Nano-scratch	Micro-scratch	Reciprocating micro-wear	Micro-impact
Wear resistance	a-C:H > Si-a-C:H > a-C:H:W	-	-	a-C:H > Si-a-C:H > a-C:H:W	a-C:H:W >> a-C:H > Si-a-C:H
Friction coefficient	a-C:H:W > Si-a-C:H > a-C:H	a-C:H:W > Si-a-C:H > a-C:H	a-C:H:W > Si-a-C:H ~ a-C:H	a-C:H > Si-a-C:H > a-C:H:W	-
L_y critical load	-	a-C:H > Si-a-C:H > a-C:H:W	a-C:H ~ Si-a-C:H ~ a-C:H:W	-	-
L_{c1} critical load	-	a-C:H:W >> Si-a-C:H ~ a-C:H	a-C:H:W > a-C:H > Si-a-C:H	-	-
L_{c2} critical load	-	-	a-C:H:W > a-C:H > Si-a-C:H	-	-

Figure captions

1. (a) Raw friction vs. sliding distance data from a test on a-C:H at 500 mN where a change from lower to higher friction occurred rapidly over a few cycles (b) example friction loops from the test before and after this transition.
2. Variation in friction coefficient with load for (a) a-C:H (b) Si-a-C:H (c) a-C:H:W.
3. Variation in friction coefficient at 500 mN for (a) a-C:H (b) Si-a-C:H (c) a-C:H:W.
4. SEM images of wear tracks at 500 mN. (a) a-C:H (b) showing partially fractured region on a-C:H (c) Si-a-C:H (d) a-C:H:W.
5. Variation of impact depth with the number of impacts for tests at 500-2000 mN (a) a-C:H; (b) Si-a-C:H; (c) a-C:H:W. Corresponding depth increases after the initial impact depth for first 30 impacts (d) a-C:H; (e) Si-a-C:H. (f) Depth increases at 1750 and 2000 mN on a-C:H:W in tests showing fracture. (g) Optical images of the arrays of multiple impact tests at 500-2000 mN on (left) a-C:H and (right) Si-a-C:H.
6. Load dependence of the mean depth after a single impact, the depth at fracture failure and final depth (a) a-C:H; (b) Si-a-C:H. (c) Load dependence of the mean depth after a single impact and final depth on a-C:H:W (d) comparison of final depth.
7. SEM images of impact craters on a-C:H. (a) 500 mN (b) 1250 mN (c) 1750 mN (d) higher magnification image of crater in (c).
8. SEM and EDX images of an impact crater on Si-a-C:H at 1750 mN.
9. SEM images of impact craters on a-C:H:W (a) 1000 mN (b) back-scattered electron image at 1750 mN.
10. Simulated von Mises stress distributions below the sliding contact for sliding at 100 mN with R = 5 μm diamond probe. Left = a-C:H; middle = Si-a-C:H; right = a-

C:H:W. Maximum and minimum von Mises stresses were 18.9-1.0 GPa for a-C:H, 13.6-0.7 GPa for Si-a-C:H and 11.5-0.5 GPa a-C:H:W. The overstressed areas (where the von Mises stress > yield stress) are shown by hashed regions. The scratch direction is left to right. The dotted line marks the coating-substrate interface.

11. Load dependence of the mean damage rate over the final 10 impacts.

Figures

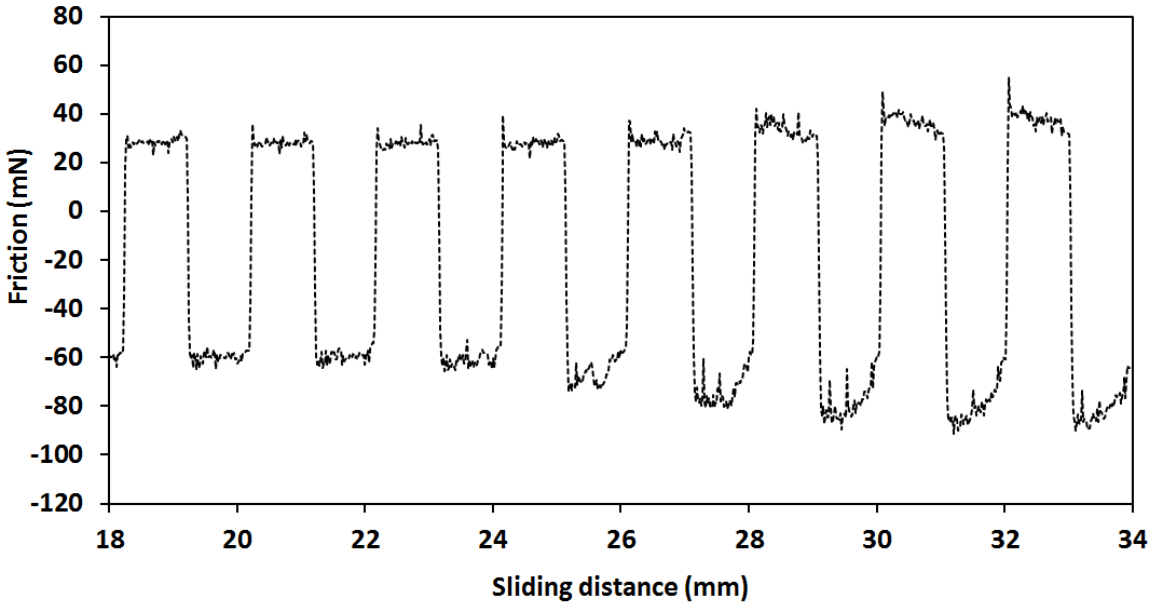

1(a)

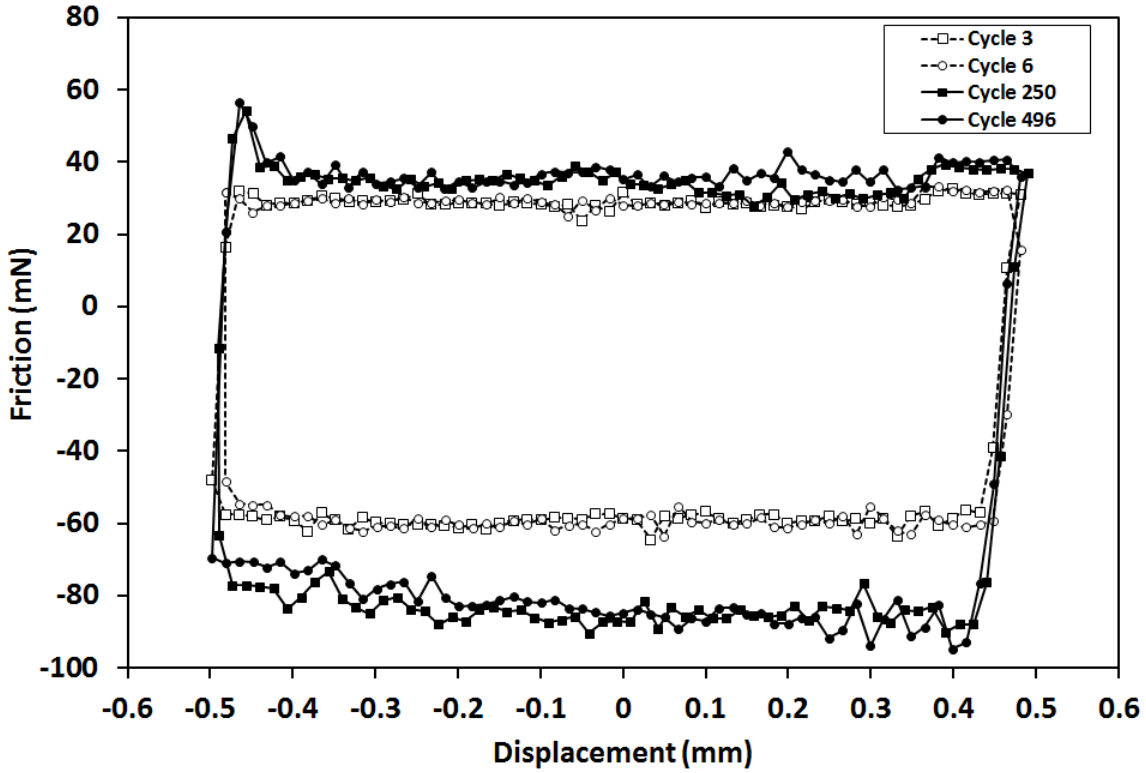
Cycle 3
Cycle 6
Cycle 250
Cycle 496
Friction (mN)
Displacement (mm)
80
60
40
20
0
-20
-40
-60
-80
-100
-0.6
-0.5
-0.4
-0.3
-0.2
-0.1
0
0.1
0.2
0.3
0.4
0.5
0.6

1(b)

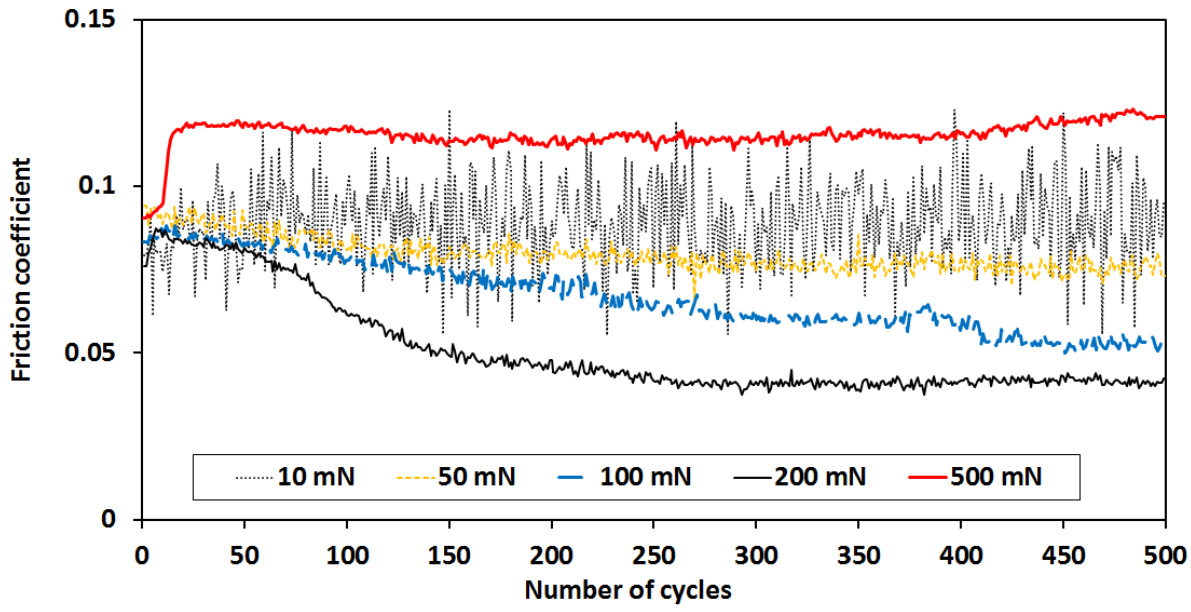
Friction coefficient
Number of cycles
10 mN
50 mN
100 mN
200 mN
500 mN
0.15
0.1
0.05
0
0
50
100
150
200
250
300
350
400
450
500

2(a)

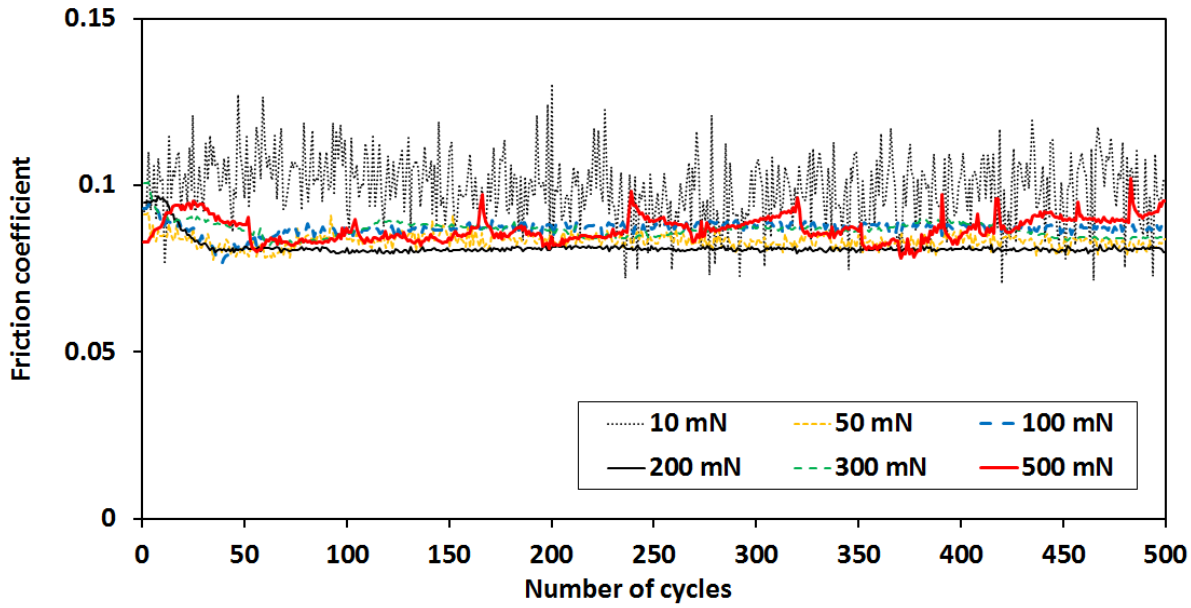
0.15
0.1
0.05
0
Friction coefficient
0
50
100
150
200
250
300
350
400
450
500
Number of cycles
10 mN
50 mN
100 mN
200 mN
300 mN
500 mN

2 (b)

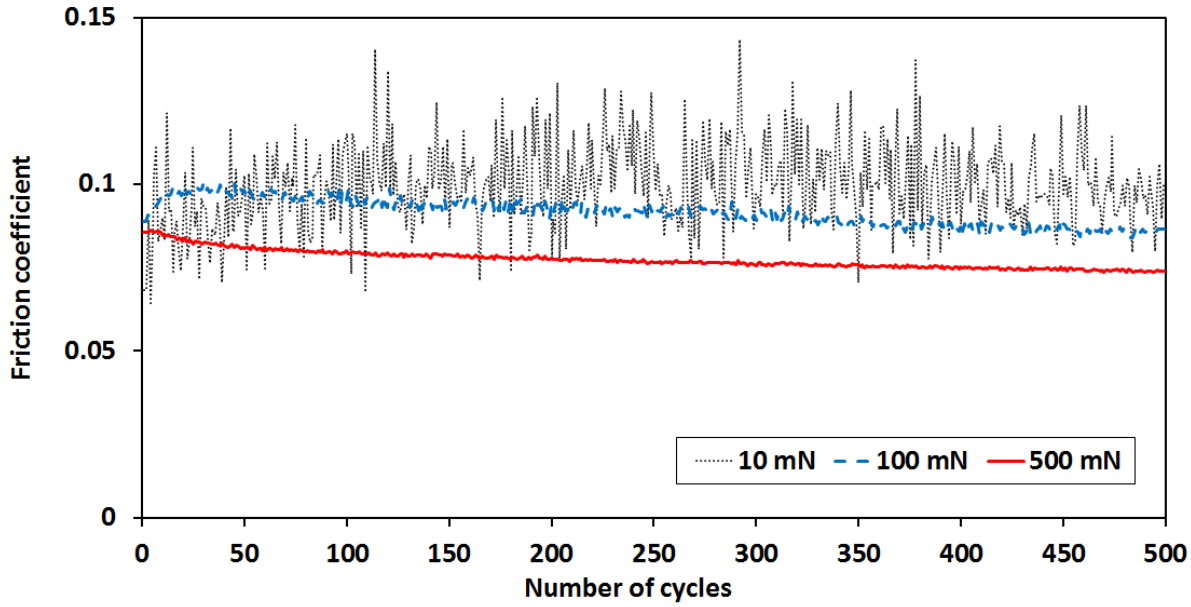
0.15
0.1
0.05
0
Friction coefficient
0
50
100
150
200
250
300
350
400
450
500
Number of cycles
10 mN
100 mN
500 mN

2 (c)

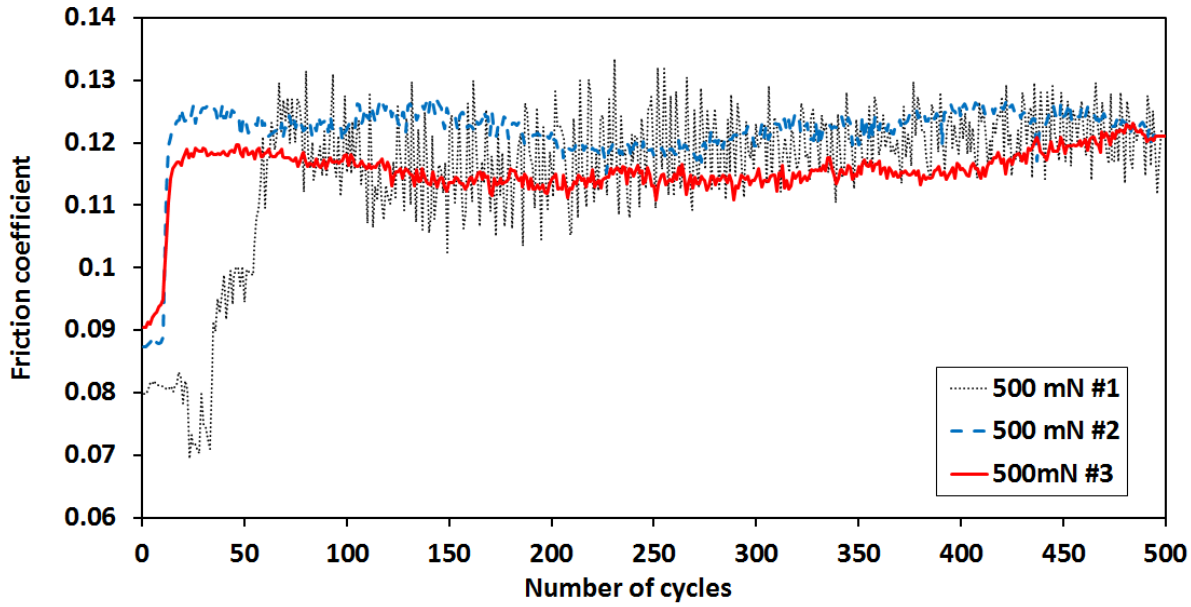
0.14
0.13
0.12
0.11
0.1
0.09
0.08
0.07
0.06
Friction coefficient
0
50
100
150
200
250
300
350
400
450
500
Number of cycles
500 mN #1
500 mN #2
500mN #3

3 (a)

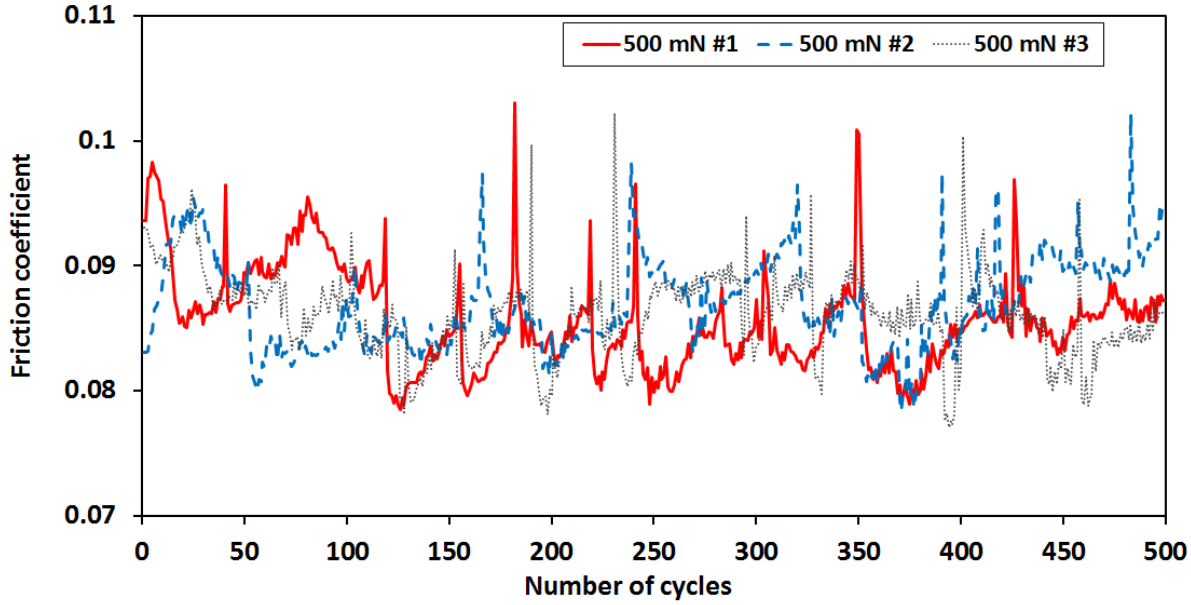
0.11
0.1
0.09
0.08
0.07
Friction coefficient
0
50
100
150
200
250
300
350
400
450
500
Number of cycles
500 mN #1
500 mN #2
500 mN #3

3 (b)

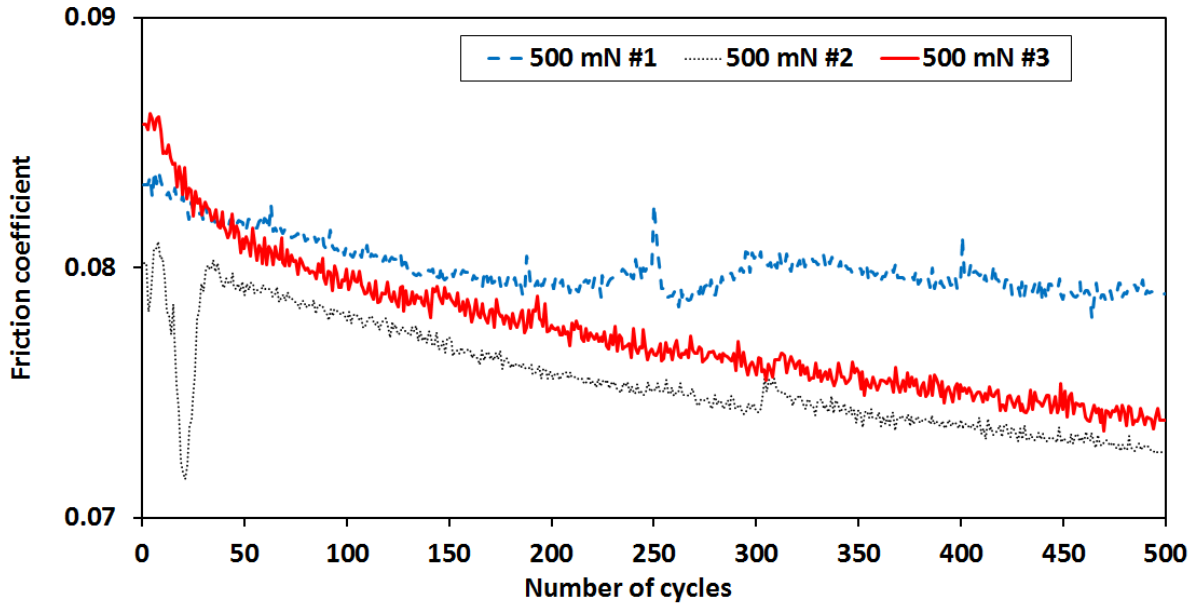
0.09
0.08
0.07
Friction coefficient
500 mN #1
500 mN #2
500 mN #3
0
50
100
150
200
250
300
350
400
450
500
Number of cycles

3 (c)

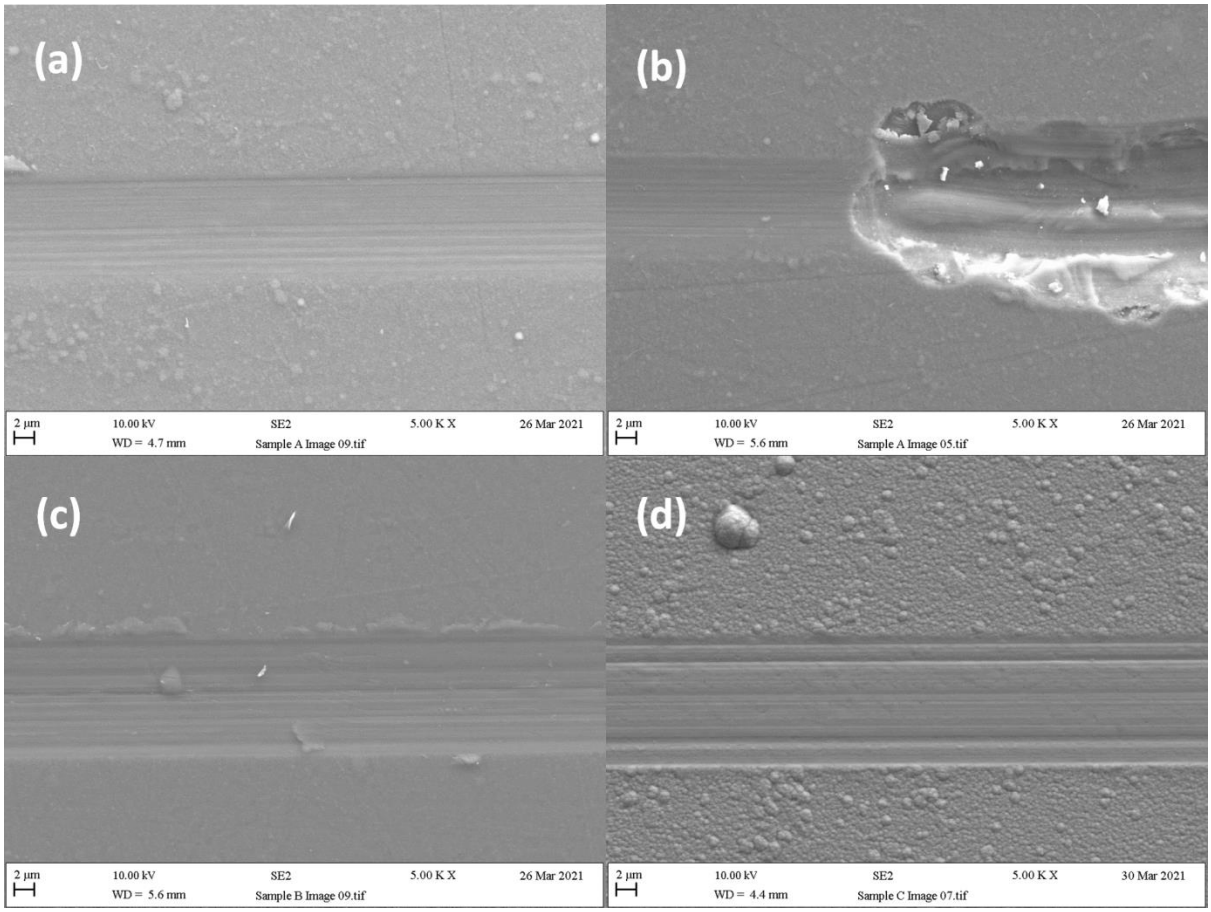
(a)
2 µm
10.00 kV
WD = 4.7 mm
SE2
Sample A Image 09.tif
5.00 K X
26 Mar 2021
(b)
2 µm
10.00 kV
WD = 5.6 mm
SE2
Sample A Image 05.tif
5.00 K X
26 Mar 2021
(c)
2 µm
10.00 kV
WD = 5.6 mm
SE2
Sample B Image 09.tif
5.00 K X
26 Mar 2021
(d)
2 µm
10.00 kV
WD = 4.4 mm
SE2
Sample C Image 07.tif
5.00 K X
30 Mar 2021

4. (a-d)

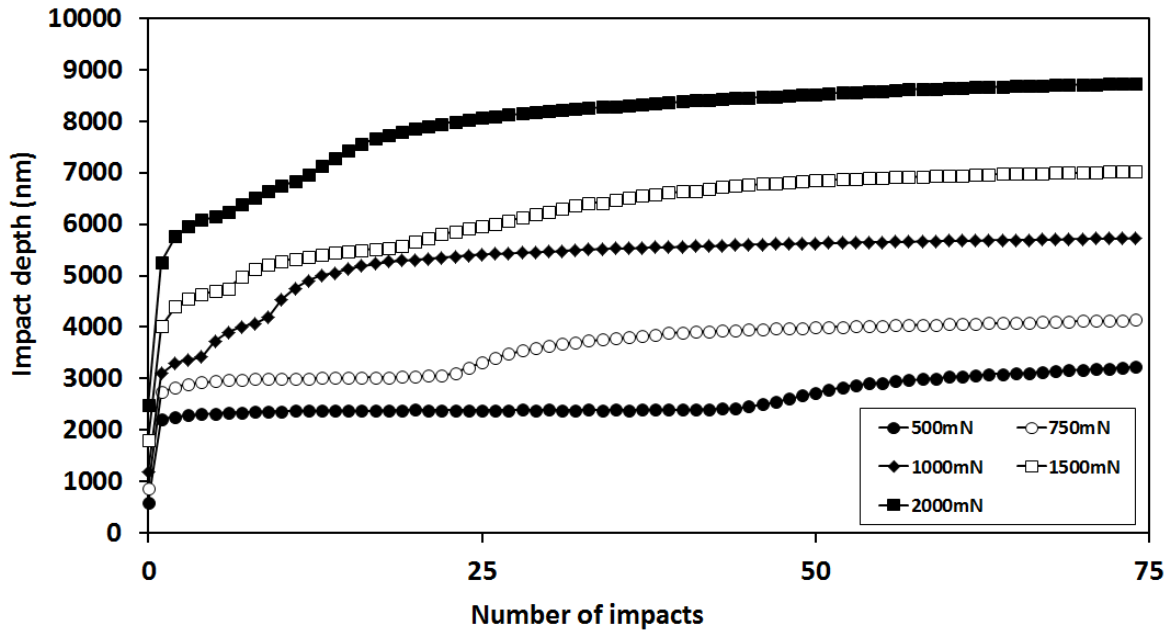
10000
9000
8000
7000
6000
5000
4000
3000
2000
1000
0
Impact depth (nm)
0
25
50
75
Number of impacts
500mN
750mN
1000mN
1500mN
2000mN

5 (a).

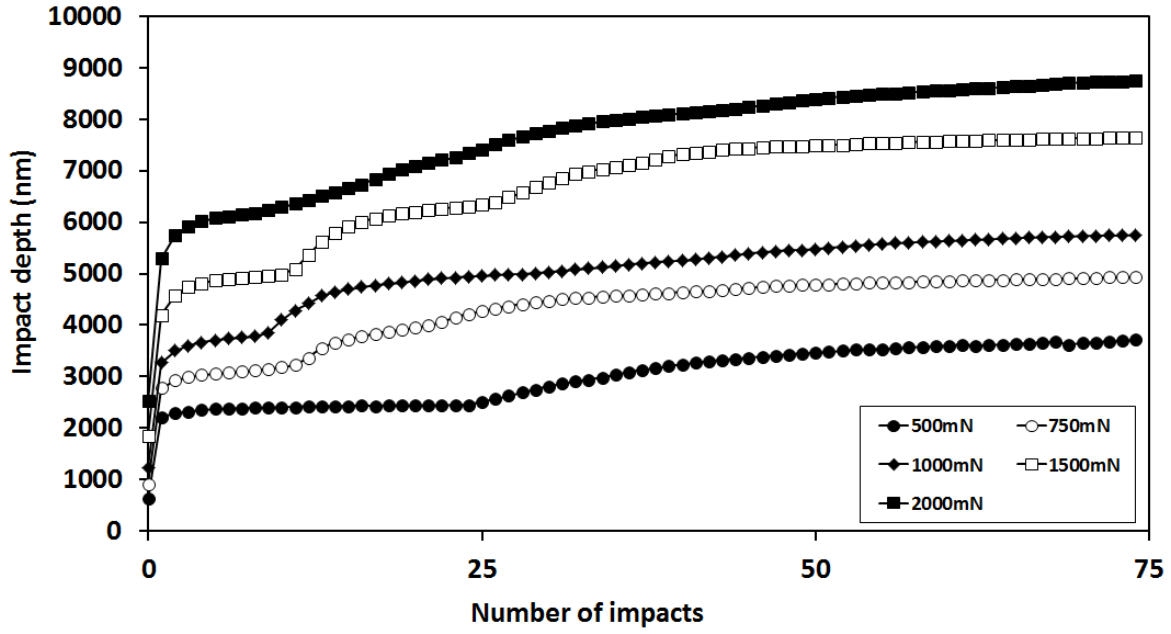
10000
9000
8000
7000
6000
5000
4000
3000
2000
1000
0
Impact depth (nm)
0
25
50
75
Number of impacts
500mN
750mN
1000mN
1500mN
2000mN

5 (b)

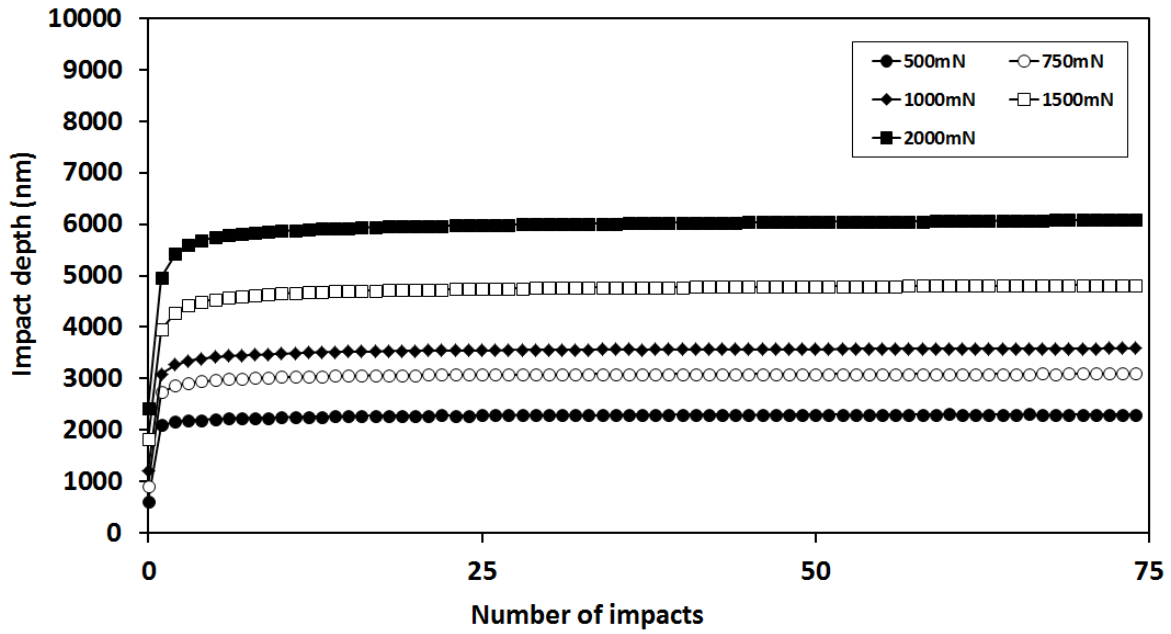
Impact depth (nm)
10000
9000
8000
7000
6000
5000
4000
3000
2000
1000
0
0
25
50
75
Number of impacts
500mN
750mN
1000mN
1500mN
2000mN

5 (c)

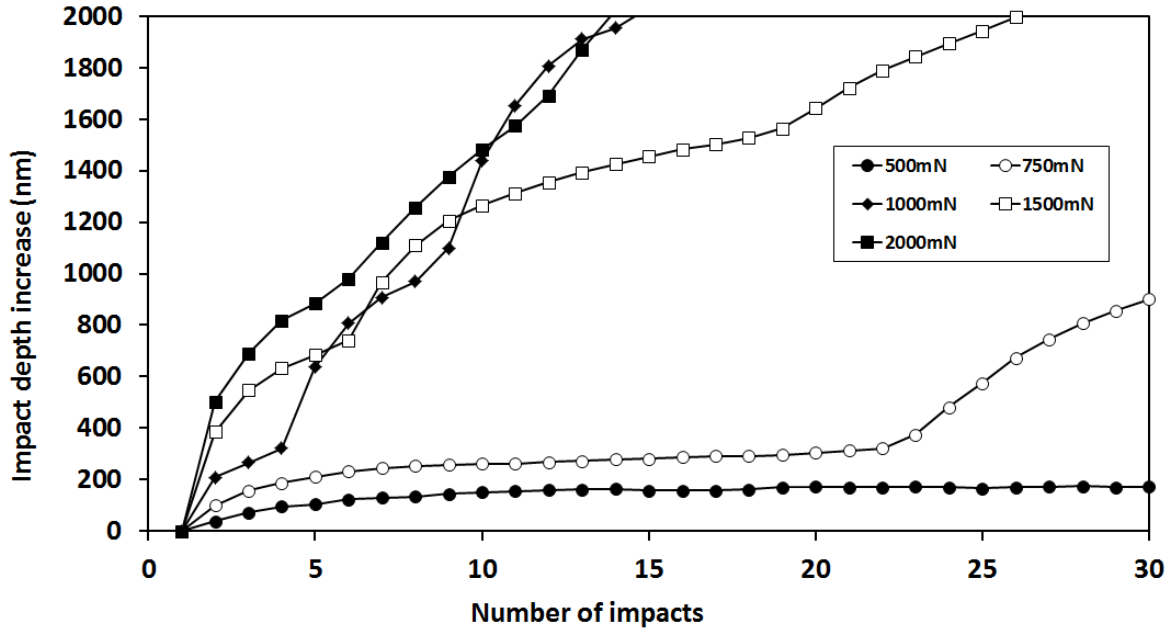
Impact depth increase (nm)
2000
1800
1600
1400
1200
1000
800
600
400
200
0
0
5
10
15
20
25
30
Number of impacts
500mN
750mN
1000mN
1500mN
2000mN

5 (d)

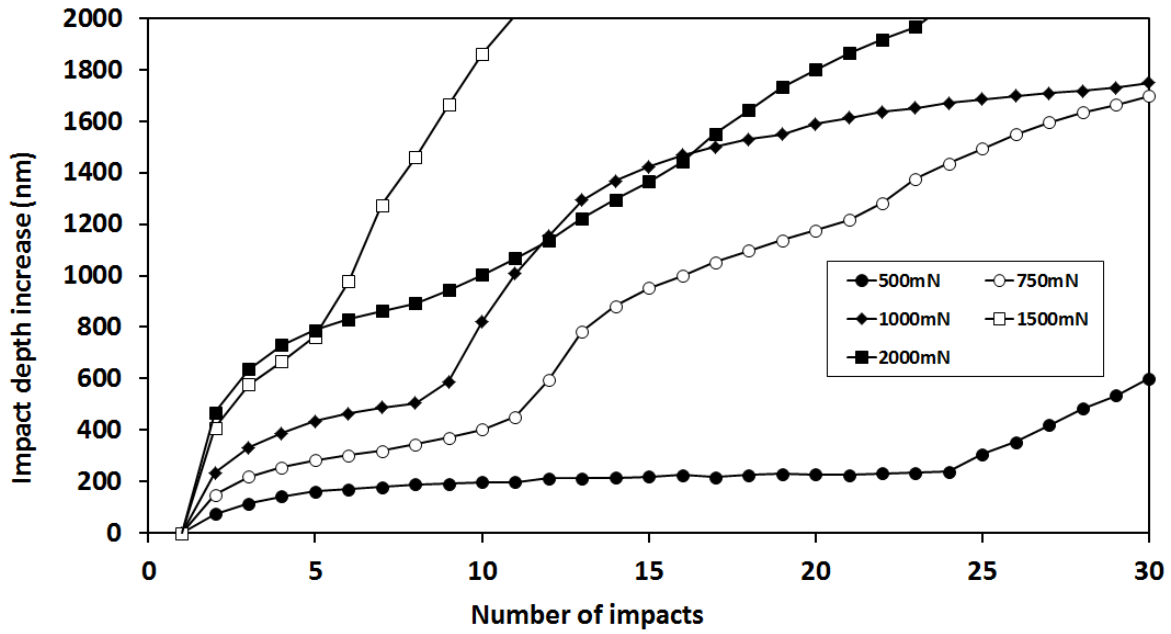
Impact depth increase (nm)
2000
1800
1600
1400
1200
1000
800
600
400
200
0
0
5
10
15
20
25
30
Number of impacts
500mN
750mN
1000mN
1500mN
2000mN

5 (e)

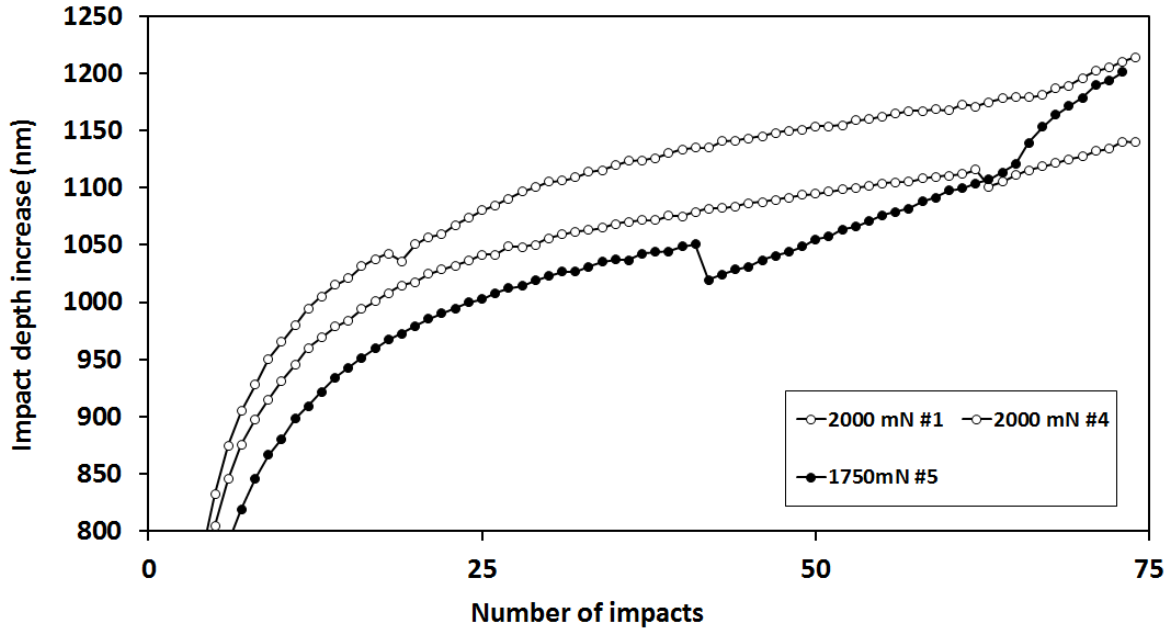
Impact depth increase (nm)
1250
1200
1150
1100
1050
1000
950
900
850
800
0
25
50
75
Number of impacts
2000 mN #1
2000 mN #4
1750mN #5

5 (f)

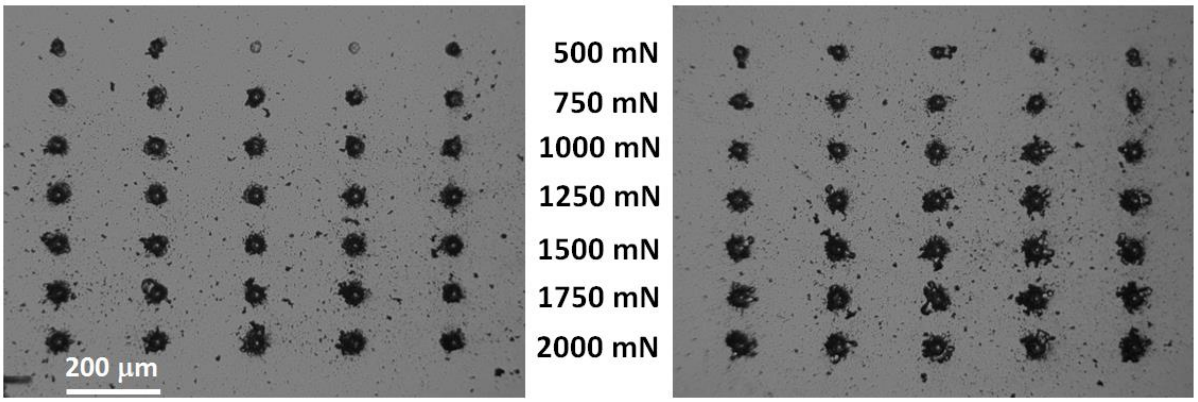
500 mN
750 mN
1000 mN
1250 mN
1500 mN
1750 mN
2000 mN
200 µm

Fig. 5 (g)

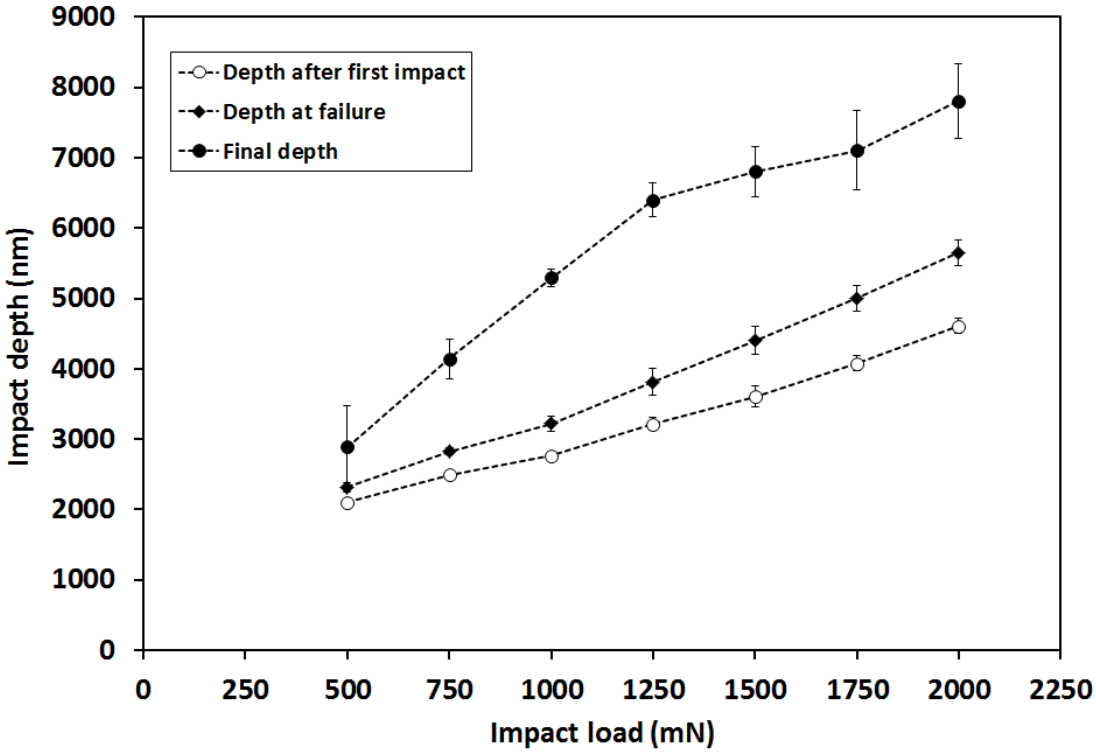
Depth after first impact
Depth at failure
Final depth
Impact depth (nm)
Impact load (mN)
0
1000
2000
3000
4000
5000
6000
7000
8000
9000
0
250
500
750
1000
1250
1500
1750
2000
2250

6 (a)

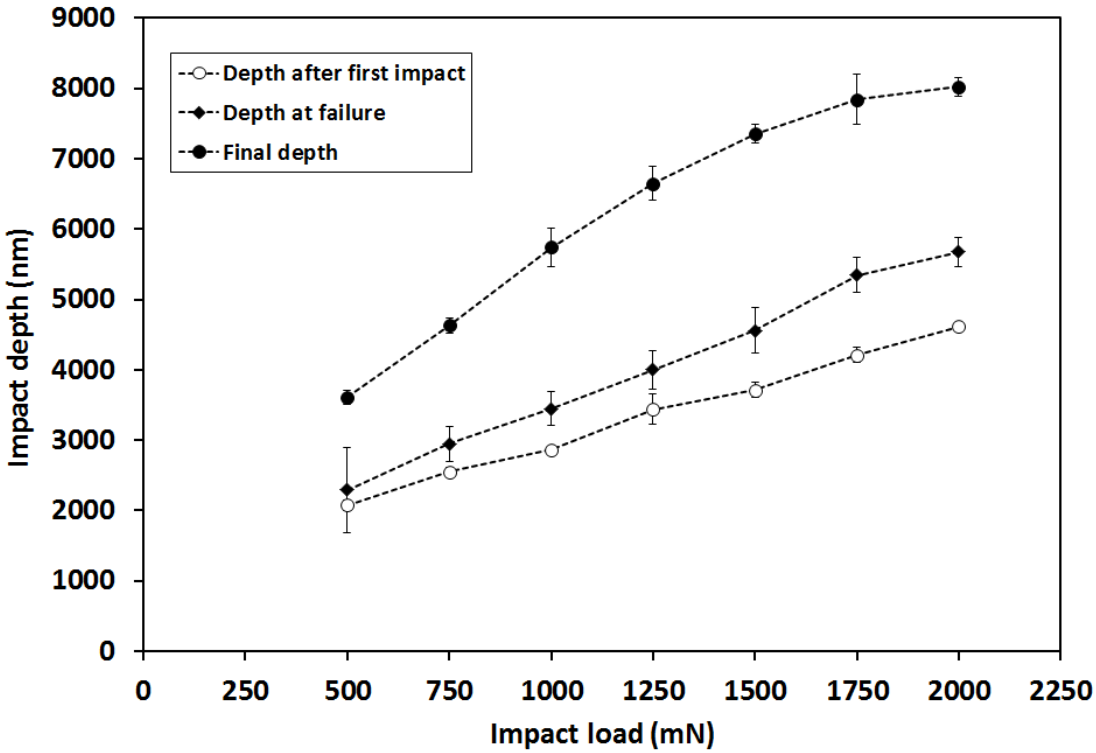
Depth after first impact
Depth at failure
Final depth
Impact depth (nm)
Impact load (mN)
0
1000
2000
3000
4000
5000
6000
7000
8000
9000
0
250
500
750
1000
1250
1500
1750
2000
2250

6 (b)

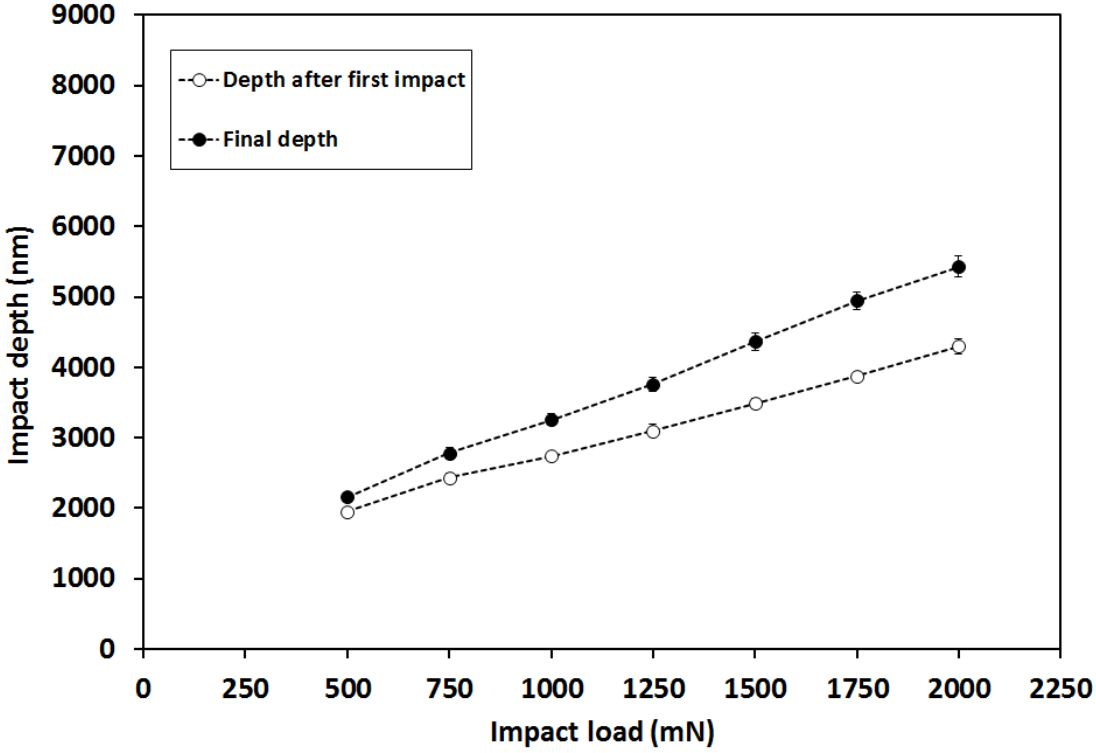
Depth after first impact
Final depth
Impact depth (nm)
Impact load (mN)
0
1000
2000
3000
4000
5000
6000
7000
8000
9000
0
250
500
750
1000
1250
1500
1750
2000
2250

6 (c)

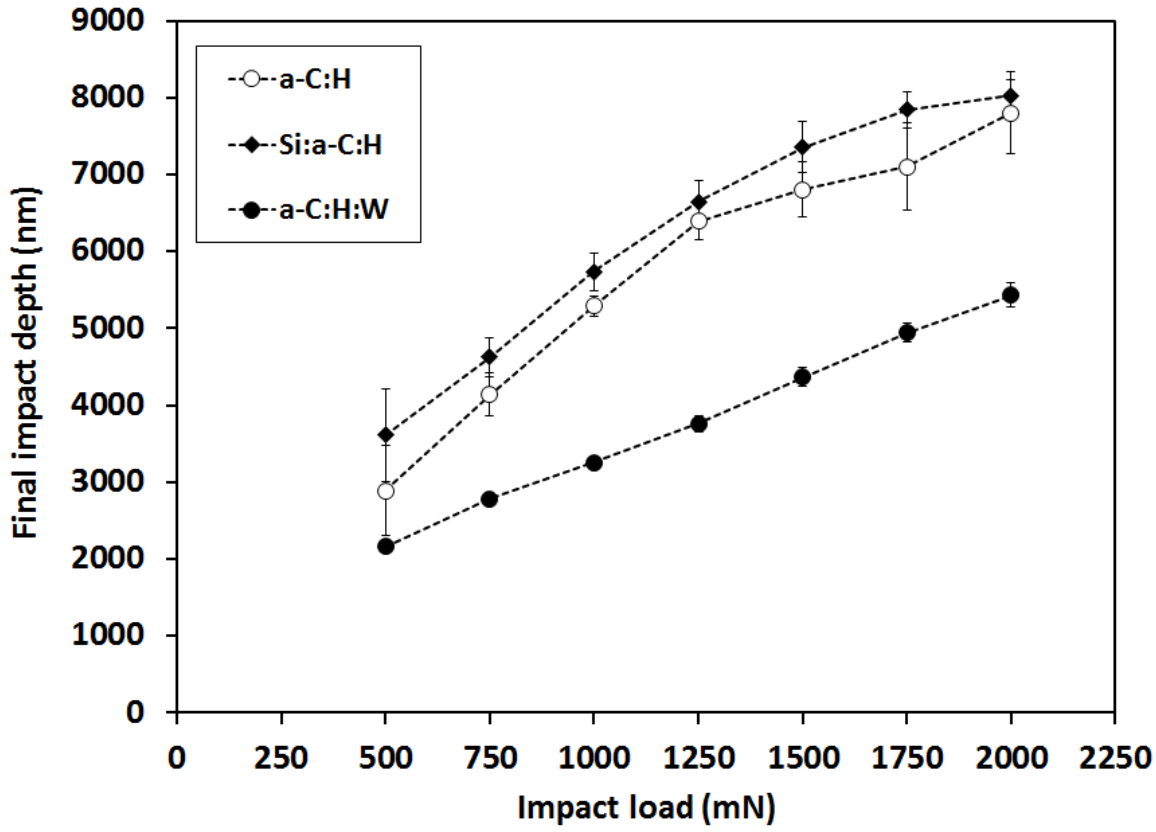
a-C:H
Si:a-C:H
a-C:H:W
Final impact depth (nm)
Impact load (mN)
0
1000
2000
3000
4000
5000
6000
7000
8000
9000
0
250
500
750
1000
1250
1500
1750
2000
2250

6 (d)

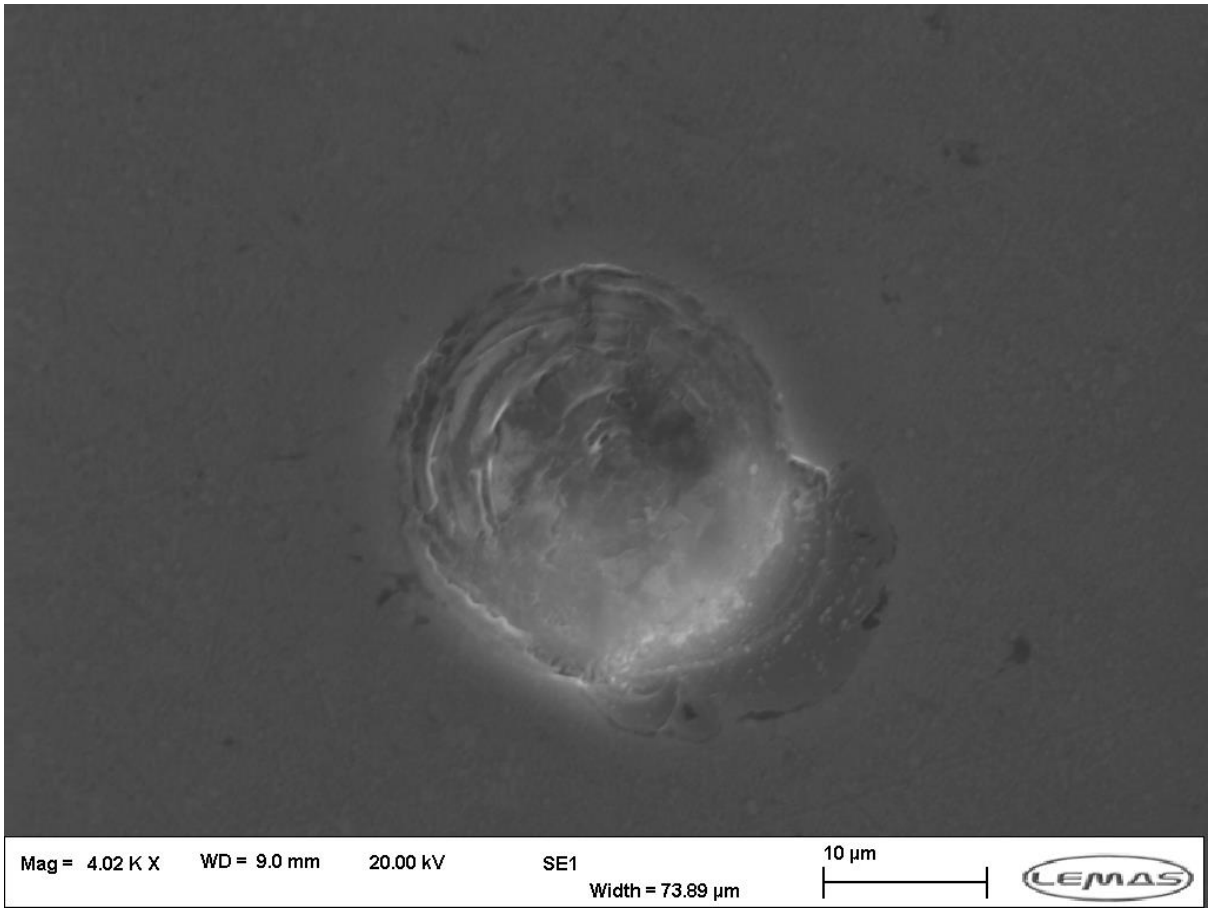

7 (a)

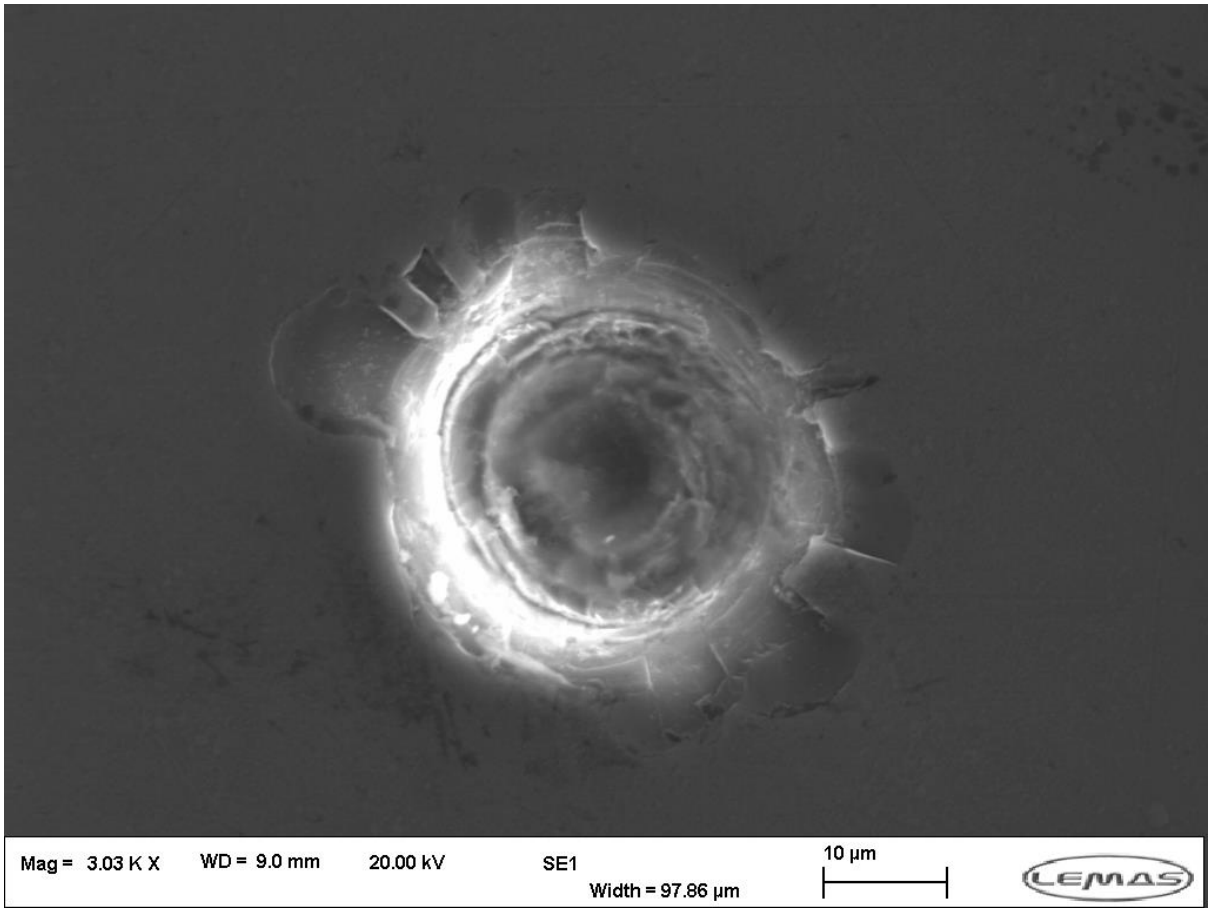

7 (b)

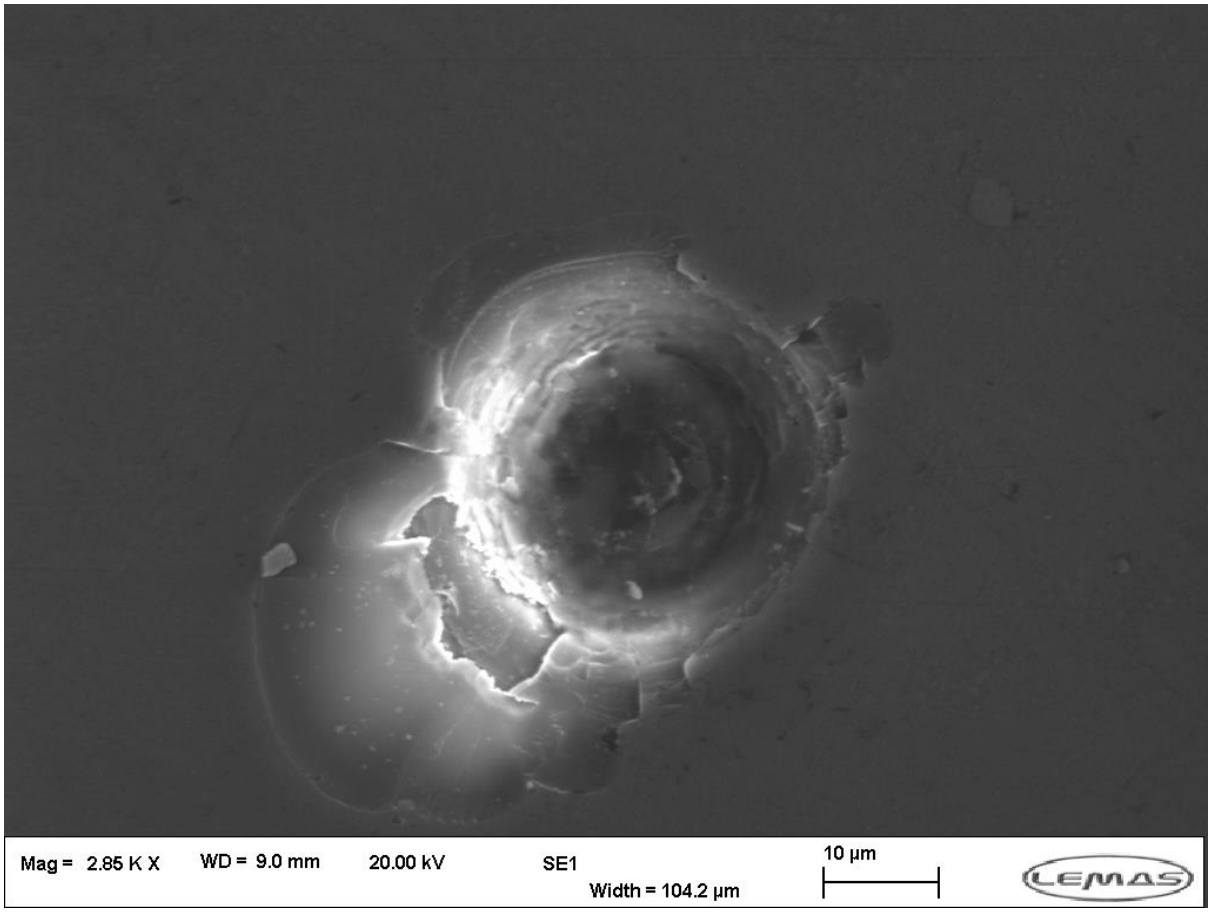

7 (c)

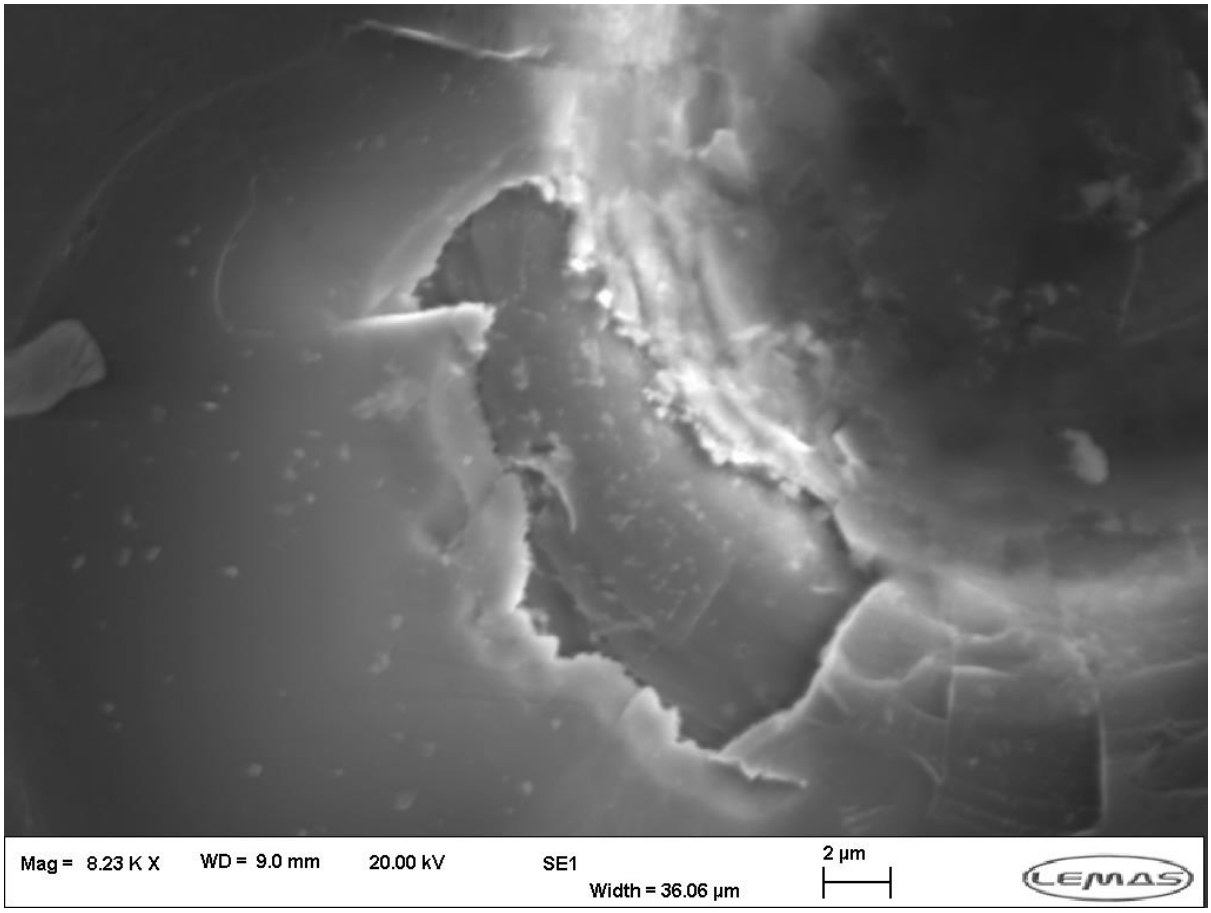
Mag = 8.23 K X
WD = 9.0 mm
20.00 kV
SE1
Width = 36.06 µm
2 µm
LEMAS

7 (d)

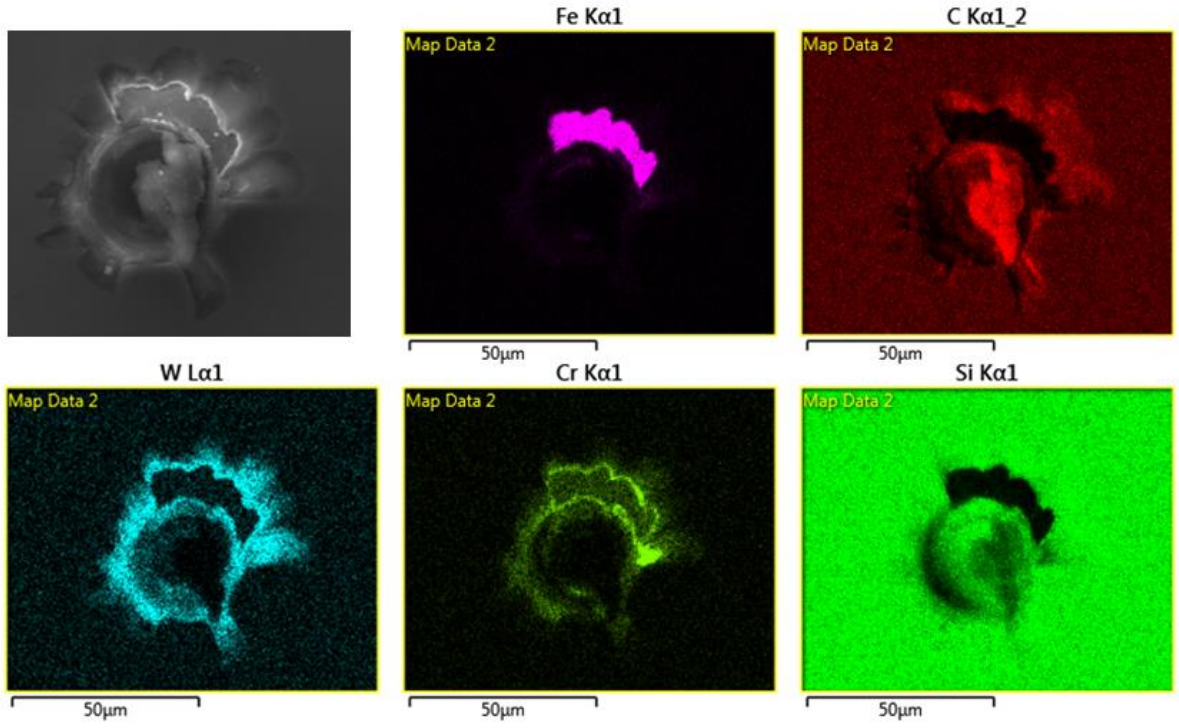
Fe Kα1
Map Data 2
50µm
C Kα1_2
Map Data 2
50µm
W Lα1
Map Data 2
50µm
Cr Kα1
Map Data 2
50µm
Si Kα1
Map Data 2
50µm

8.

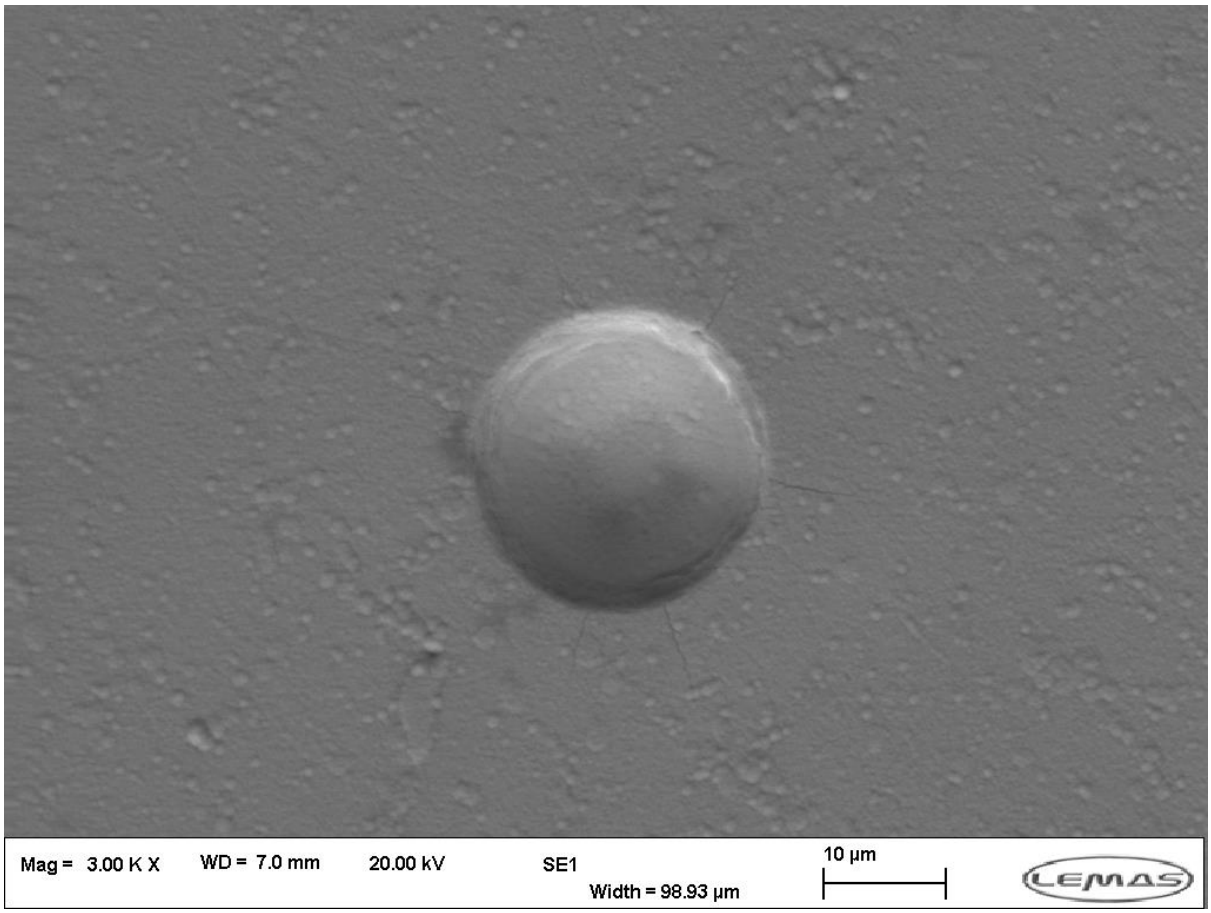

9 (a)

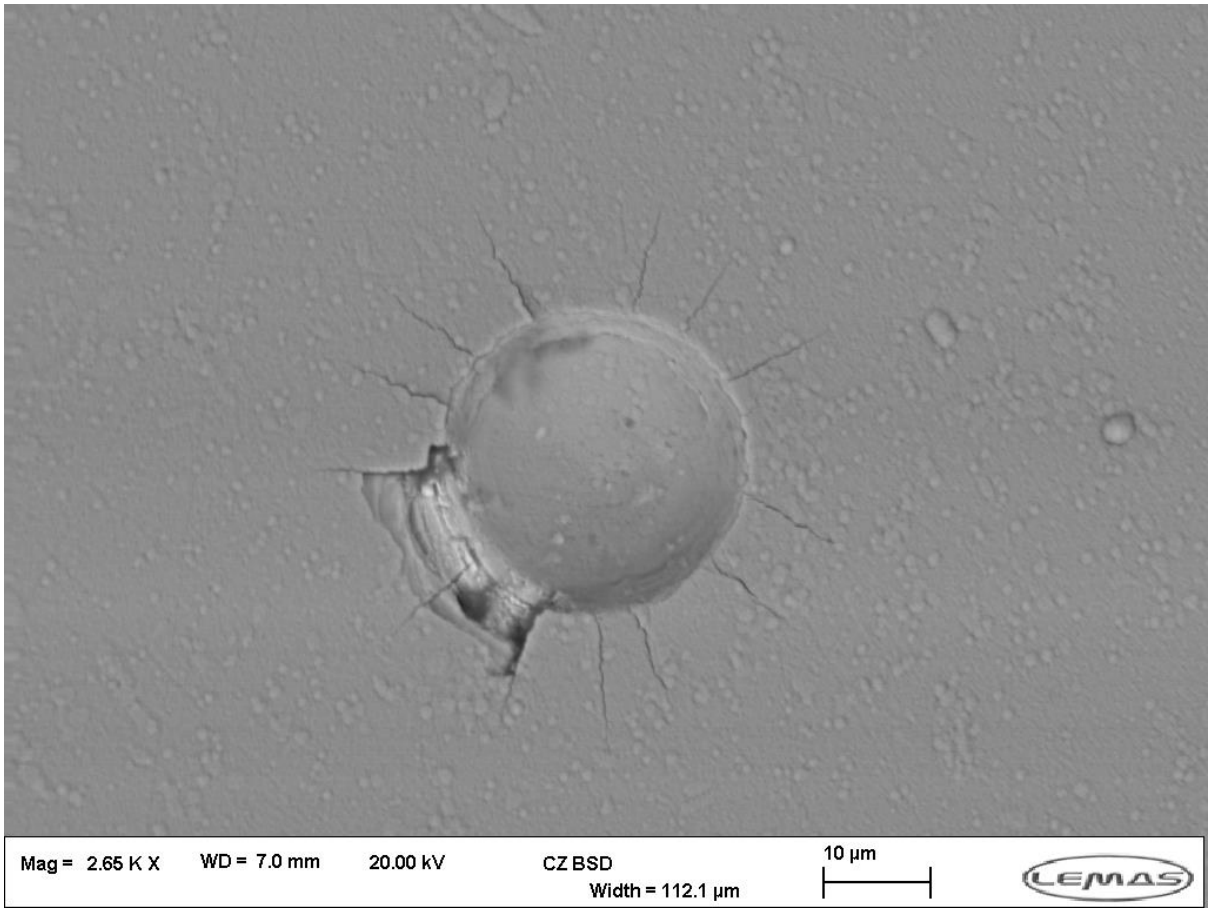
Mag = 2.65 K X
WD = 7.0 mm
20.00 kV
CZ BSD
Width = 112.1 µm
10 µm
LEMAS

9 (b)

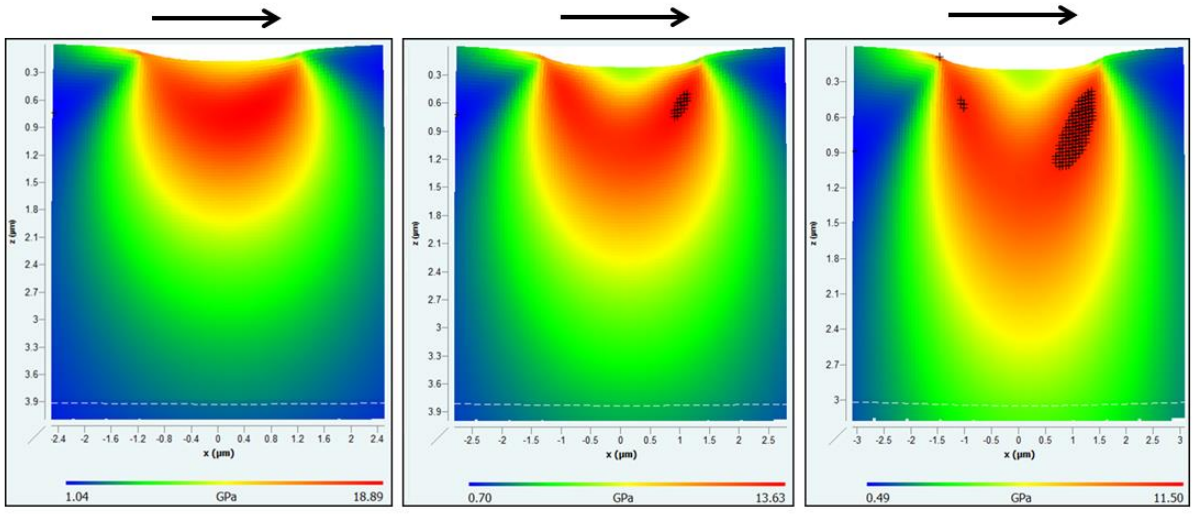
1.04
GPa
18.89
0.70
GPa
13.63
0.49
GPa
11.50

10.

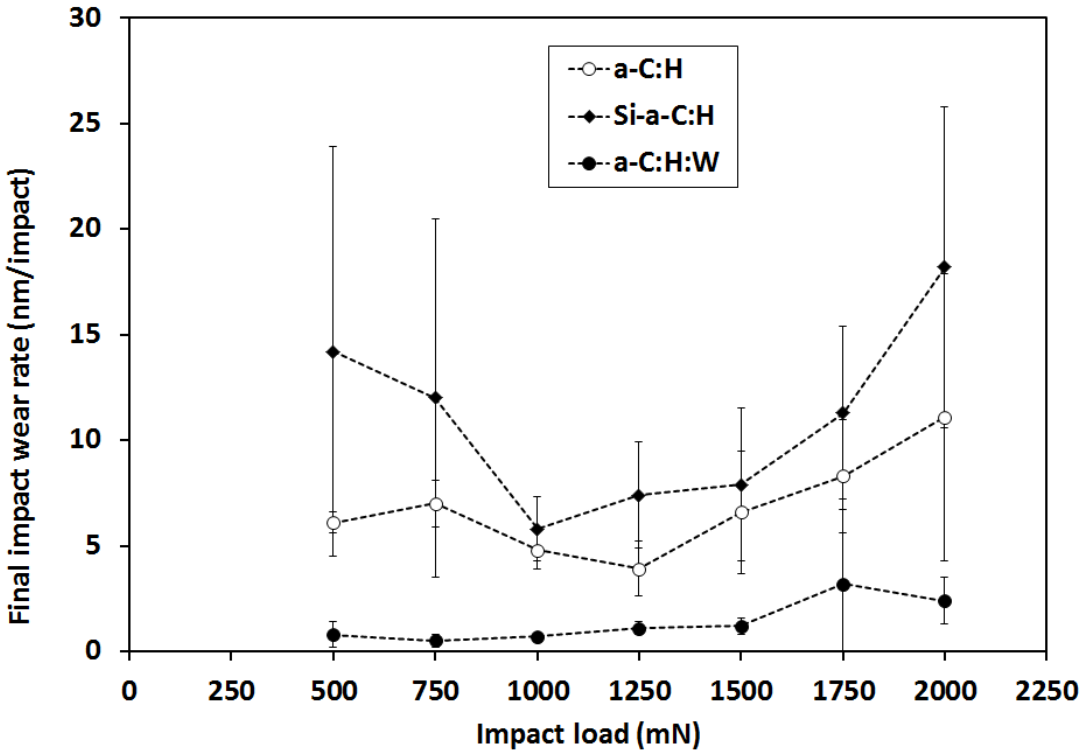
a-C:H
Si-a-C:H
a-C:H:W
Final impact wear rate (nm/impact)
Impact load (mN)
0
5
10
15
20
25
30
0
250
500
750
1000
1250
1500
1750
2000
2250

11.